Journal of Controlled Release 293 (2019) 48–62

Contents lists available at ScienceDirect

Journal of Controlled Release

journal homepage: www.elsevier.com/locate/jconrel

Modular core-shell polymeric nanoparticles mimicking viral structures for vaccination

Bo Lou[a], Ans De Beuckelaer[b], Eger Boonstra[a], Dandan Li[a], Bruno G. De Geest[c], Stefaan De Koker[b], Enrico Mastrobattista[a], Wim E. Hennink[a,*]

[a] Department of Pharmaceutics, Utrecht Institute for Pharmaceutical science, Utrecht University, 3584CG Utrecht, the Netherlands
[b] Laboratory of Molecular Immunology, Department of Biomedical Molecular Biology, Ghent University, 9052 Zwijnaarde, Belgium
[c] Department of pharmaceutics, Ghent University, 9000 Ghent, Belgium

ARTICLE INFO

Keywords:
Nanoparticles
Vaccine adjuvant
TLR7/8
Virus mimicking structure
Click chemistry

ABSTRACT

Recent advances in the development of protein-based vaccines have expanded the opportunities for preventing and treating both infectious diseases as well as cancer. However, the development of readily and efficient antigen delivery systems capable of stimulating strong cytotoxic T-lymphocyte (CTL) responses remains a challenge. With the attempt to closely mimic the properties of viruses in terms of their size and molecular organization, we constructed RNA (which is a ligand for Toll-like receptor 7 (TLR7) and TLR8) and antigen-loaded nanoparticles resembling the structural organization of viruses. Cationic polymers containing either azide or bicyclo[6.1.0]nonyne (BCN) groups were synthesized as electrostatic glue that binds negatively charged single stranded RNA (PolyU) to form a self-crosslinked polyplex core. An azide-modified model antigen (ovalbumin, OVA) and a BCN-modified mannosylated or galactosylated polymer were sequentially conjugated to the RNA core *via* disulfide bonds using copper free click chemistry to form the shell of the polyplexes. The generated reducible virus mimicking particles (VMPs) with a diameter of 200 nm and negatively surface charge (−14 mV) were colloidally stable in physiological conditions. The immunogenicity of these VMP vaccines was evaluated both *in vitro* and *in vivo*. The surface mannosylated VMPs (VMP-Man) showed 5 times higher cellular uptake by bone marrow derived DCs (BMDCs) compared to galactosylated VMP (VMP-Gal) counterpart. Moreover, VMP-Man efficiently activated DCs and greatly facilitated MHC I Ag presentation *in vitro*. Vaccination of mice with VMP-Man elicited strong OVA-specific CTL responses as well as humoral immune responses. These results demonstrate that the modular core-shell polymeric nanoparticles described in this paper are superior in inducing strong and durable immune responses compared to adjuvanted protein subunit vaccines and offer therefore a flexible platform for personalized vaccines.

1. Introduction

Protein subunit vaccines have been extensively investigated as a safe alternative to classical vaccines consisting of whole, attenuated or inactivated pathogens [1]. Also for cancer immunotherapy, vaccines based on tumor-associated antigens or tumor neoantigens are being explored [2–4]. Recombinant or purified protein antigens for vaccination have a good safety profile and have been extensively tested in clinical studies [5,6]. However, protein subunit vaccines as such are poorly immunogenic [7]. Thus, the inclusion of an adjuvant in the vaccine formulation is necessary to induce a more potent immune response. The mostly used adjuvants in clinical trials are emulsions (*e.g.* AS03 and MF59®), which can enhance the antigen persistence at the injection site and increase recruitment and activation of antigen presenting cells (APCs). Nonetheless, repeated immunization can cause antigen-specific T cell sequestration, dysfunction and deletion [8], and is also associated with the risk to induce autoimmunity [9].

Alternatively, nanoparticles have been used to adjuvant protein vaccine formulations [10,11]. The use of nanoparticles in vaccinology is inspired by the fact that most pathogens have a dimension within the sub-micron size range, and can therefore be processed efficiently by the immune system, leading to a potent immune response. One of the most intensively studied polymer-based protein delivery systems are biodegradable poly(lactic-*co*-glycolic acid) (PLGA) nanoparticles [12–14]. The co-delivery of Toll-like receptor ligands (TLRs) and protein antigens in PLGA particles can efficiently induce strong $CD8^+$ T cell

* Corresponding author.
E-mail address: W.E.Hennink@uu.nl (W.E. Hennink).

https://doi.org/10.1016/j.jconrel.2018.11.006
Received 28 July 2018; Received in revised form 23 October 2018; Accepted 4 November 2018
Available online 11 November 2018
0168-3659/

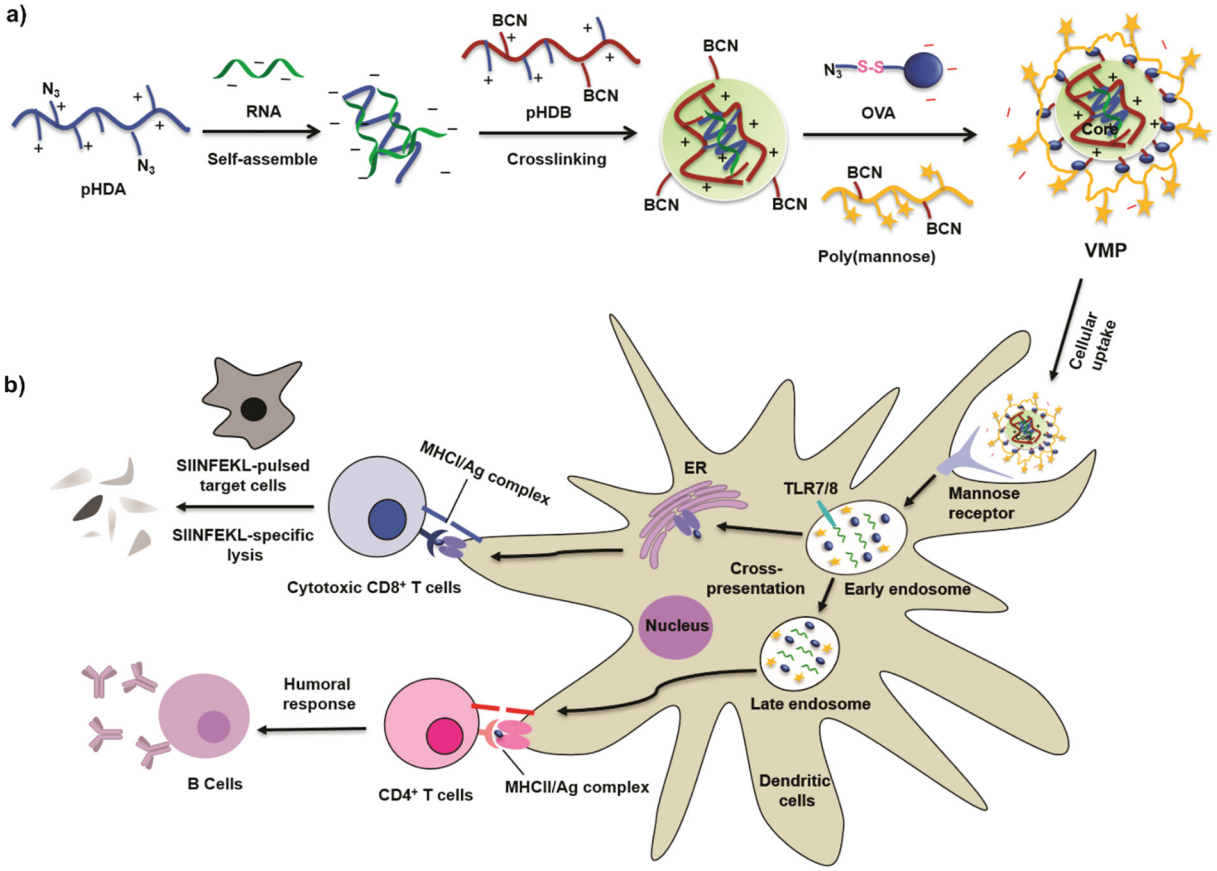

Scheme 1. Design of synthetic virus mimicking particles (VMPs) vaccines. (a) Schematic illustration of sequential assembly of VMP particles. pHDA: cationic polymer containing azide groups; pHDB: cationic polymer containing cyclooctyne groups (bicyclo[6.1.0]nonyne (BCN)). (b) The VMP particles specifically target to dendritic cells, promote antigen cross-presentation, and induce DC maturation, resulting in elicitation of robust antigen-specific cytotoxic T lymphocytes responses and superior antibody production.

responses to inhibit the growth of tumors or to protect against a viral challenge [15,16]. Besides PLGA, a whole spectrum of different nanocarriers systems, both polymeric as well as lipidic, has been developed for vaccination purposes, with most of these systems relying on the entrapment of antigens in the core of the nanoparticles to efficiently deliver their loading to antigen presenting cells [17–20]. The pharmaceutical limitation of this approach is that one needs to empirically optimize the vaccine formulation in terms of encapsulation efficiency and antigen release, which is often time consuming with different requirements for different antigens. For this reason, the encapsulation approach is not recommended for manufacturing of personalized vaccines.

Here, we propose an alternative and simple strategy to produce antigen and adjuvant loaded nanoparticles by using synthetic biodegradable polymers (Scheme 1). Our strategy is based on the formation of a universal nanoparticle with a crosslinked core containing virus-mimicking single chain RNA (PolyU) as TLR-adjuvant to which different layers of functional shells (*e.g.* antigen and stabilizer poly(mannose)) can be coupled using copper-free click chemistry (Scheme 1a). Such modular core-shell polymeric nanoparticles resemble viruses in terms of size and supramolecular organization and as such are expected to efficiently boost the immune system. Virus-mimicking nanoparticles (VMPs) were constructed by sequential self-assembly of single stranded RNA (adjuvant), ovalbumin (as model antigen) with cationic polymers and stabilized with poly(mannose) for targeting the mannose-receptors on the surface of DCs [21]. VMPs surface modified with poly(galactose) were prepared as a negative control, as galactose has very low binging affinities for mannose receptors. The strength of this vaccine delivery system lies in the flexibility at which different antigen shell layers can be "clicked" onto the VMP core, enabling versatile adaptation for different vaccine application. As the antigen is covalently linked to the RNA core, antigen loading becomes independent on the properties of antigen used. To ensure antigen release once delivered into antigen presenting cells, reducible disulfide bonds were introduced between the polymeric shell and the antigen, enabling intracellular antigen release [22–24]. These VMPs were tested for antigen-specific immune activation both *in vitro* and *in vivo* and showed robust antigen-specific immune activation that warrants its further investigation as a modular vaccine platform.

2. Materials and methods

2.1. Materials

Imidazole-1-sulfonyl azide hydrochloride [25], N-(2-hydroxyl propyl)-methacrylamid (HPMA) and DMAE-CI [26] were synthesized as previously described. Azobis(isobutyronitrile) (AIBN), 4-cyano-4-[(dodecylsulfanylthiocarbonyl)sulfanyl]pentanoic acid (CDTPA), azidoacetic acid N-hydroxysuccinimide ester, acrylic acid N-hydroxysuccinimide ester (NAS) and all other reagents and solvents used were obtained from Sigma (Zwijndrecht, the Netherlands) and were used without further purification. 2,5-Dioxopyrrolidin-1-yl 4-((((1R,8S,9s)-bicyclo [6.1.0] non-4-yn-9-ylmethoxy)carbonyl)amino) butanoate (BCN, SX-A1036) was purchased from Synaffix BV (Oss, the Netherlands). Ovalbumin (OVA) and PolyU were purchased from InvivoGen (Toulouse, France). Cy5-mRNA_luc was from Teu-bio (TRiLink biotechnologies, San Diego, USA). Agarose multi-purpose was purchased from Roche Molecular Biochemicals (Mannheim, Germany). 6×

DNA Loading Dye was purchased from Fermentas (St. Leon-Roth, Germany). SYBR Safe DNA gel stain, Dulbecco's phosphate buffered saline (DPBS), RPMI-1640/IMDM medium, Opti-MEM, and heat inactivated fetal bovine serum (HI-FBS) were purchased from Life Technologies (Breda, the Netherlands).

2.2. Monomer synthesis

2.2.1. Synthesis of 1,2-bis(2-azidoethyl) disulfane

The synthesis procedures were similar as the methods described above (Scheme S1). Typically, imidazole-1-sulfonyl azide hydrochloride chloride salt (5.0 g, 23.9 mmol) was added to cystamine dihydrochloride salt (2.2, 9.9 mmol), K_2CO_3 (6.1 g, 44.2 mmol) and $CuSO_4{\cdot}5H_2O$ (59.6 mg, 238.5 μmol) in methanol (100 mL) and the mixture was stirred at room temperature for 12 h. Next, the mixture was concentrated, diluted with H_2O (200 mL), and extracted with DCM (3 × 100 mL). The combined organic layers were dried ($MgSO_4$), filtered and concentrated. Flash chromatography gave the aimed product as a yellow oil (DCM/MeOH/NH_4OH, 3/1/0.1). The yield was 1.9 g (94%, R_f = 0.5). The monomer was characterized by ^{1}H NMR spectroscopy (Fig. S4).

2.2.2. Synthesis of 3-((2-azidoethyl) disulfanyl) propanoic acid NHS ester (ADDP)

The synthesis procedure of 3-((2-azidoethyl)disulfanyl)propanoic acid was based on a previous study (Scheme S2) [27]. In detail, 1,2-bis (2-azidoethyl) disulfane (1.9 g, 9.3 mmol) was dissolved in methanol (100 mL) and cooled in an ice bath. A solution of 3-chloroperbenzoic acid (mCPBA, Sigma-Aldrich, the Netherlands) (75%, 2.6 g, 11.2 mmol) in DCM (20 mL) was added dropwise. The reaction mixture was stirred overnight at room temperature and the solvent was subsequently evaporated *in vacuo* to give a white residue. The obtained solid was suspended in methanol (50 mL), to which dropwise 3-mercaptopropionic acid (0.81 mL, 9.3 mmol) was added. The resulting solution was stirred overnight at room temperature. The solvent was removed *in vacuo* and the resulting oil was purified by basic Al_2O_3 gel, eluted with MeOH/$CHCl_3$/AcOH = 10/100/1. The aimed compound was obtained as a pale yellow oil. The yield was 1.4 g (75%, R_f = 0.4) and characterized by ^{1}H NMR spectroscopy (400 MHz, DMSO-d_6) (Fig. S5).

Next, 3-((2-azidoethyl) disulfanyl) propanoic acid was activated with NHS. Briefly, 1.0 g of 3-((2-azidoethyl) disulfanyl) propanoic acid (4.8 mmol) and 0.9 mg of N-hydoxysuccinimide (NHS, 7.2 mmol) were dissolved in 15 mL DCM. Then, 1.5 g of dicyclohexylcarbodiimide (DCC, 7.2 mmol) was added and the mixture was stirred overnight at room temperature. After filtration of insoluble dicyclohexylurea (DCU) and evaporation of DCM, the mixture was purified using a silica gel column (DCM/MeOH = 50/2, *v*/v). The yield was 0.9 g (59%, R_f = 0.8) and the product was characterized by ^{1}H NMR spectroscopy (400 MHz, DMSO-d_6) (Fig. S6).

2.2.3. Synthesis of 3-(2-aminoethylthio) propyl α-D-mannopyranoside/galactopyranoside (Man-NH_2/Gal-NH_2)

The reaction consists of elongation of the alkyne group of allyl α-D-mannopyranoside/galactopyranoside (Sigma-Aldrich, the Netherlands) by adding 2-aminoethanethiol according to reaction Scheme S3 [28]. Typically, 1,2 g of allyl α-D-mannopyranoside (5.5 mmol) was dissolved in 2 mL deoxygenated water in which 570 mg of cysteamine hydrochloride (5.0 mmol) was also dissolved. The solution was then irradiated with UV light of 254 nm for 17 h to accelerate the reaction. Next, the solution was diluted with 100 mL methanol and dried ($MgSO_4$), filtered and concentrated. The resulting oil residue was purified by silica gel chromatography (MeOH/NH_4OH, 100:1), to give final product Man-NH_2 as a colorless oil (1.2 g, 73%, R_f = 0.25). The products were characterized by the ^{1}H NMR spectroscopy (Fig. S11).

2.3. Synthesis of the polymers

2.3.1. Synthesis of p(HPMA-r-NAS) (pHN) by RAFT

p(HPMA-r-NAS) was synthesized by reversible addition fragmentation chain transfer (RAFT) copolymerization as previously published [29]. Briefly, 4-cyano-4-[(dodecyl-sulfanyl-thiocarbonyl)sulfanyl] pentanoic acid (CDTPA) was used as chain transfer agent (CTA), and AIBN as initiator (I). The polymer was synthesized using monomers (HPMA and NAS) to chain transfer agent and initiator ratio (M/CTA/I) of 100/1/0.1 (mol/mol/mol) and at a feed ratio HPMA/NAS of 70/30 (mol/mol). 1,3,5-Trioxane (Sigma-Aldrich, the Netherlands) was added as internal NMR standard with a final concentration of 0.1 M. The polymerization was carried at 70 °C for 9 h in dry DMF under argon after purging for half an hour, using a final total monomer concentration of 1.0 M. After polymerization, the conversion of the monomers was determined by ^{1}H NMR analysis by dilution (10×) a sample of the reaction mixture with DMSO-d_6. The product was precipitated into a mixture of anhydrous acetone and diethyl ether (50/50 *v*/v). To remove the trithiocarbonate end group [30], the polymer and AIBN (50 times excess, mol/mol) were dissolved in anhydrous DMF and purged with argon. The solution was heated at 80 °C for 90 min, and the polymer was subsequently precipitated in 100 mL of anhydrous acetone, collected by centrifugation. The procedure was repeated for three times and the polymer was dried under vacuum for 24 h prior to ^{1}H NMR and GPC analysis (yield: 55%, M_n = 15 kDa, M_w/M_n = 1.43). ^{1}H NMR (400 MHz, DMSO-d_6); δppm; 0.95–1.52 (backbone–CH_3, $CH_3CH(OH)$), 1.55–2.41 (backbone CH_2, backbone–CH),3.00–3.33 (CH_2NH), 3.5 (NHS–CH_2), 3.90 (CHOH).

2.3.2. Synthesis of p(HPMA-DMAE-r-AEDA) (pHDA) and p(HPMA-DMAE-r-BCN) (pHDB)

Hundred mg of the copolymer p(HPMA-r-NAS) (pHN) (0.19 mmol of NAS, 0.48 mmol of HPMA) was dissolved in 1 mL dry DMSO and purged with argon for 30 min. After that, 40 mg of 2-((2-azidoethyl) disulfanyl) ethan-1-amine hydrochloride (AEDA) or 73 mg (0.22 mmol) of BCN-amine (A-10004, Synaffix BV) was added to this solution under argon purge. Subsequently 113 mg (1.12 mmol) of triethylamine was injected into the reaction vessel and the solution was stirred at 40 °C. After 48 h, 28 mg (0.37 mmol) of d,l-amino-2-propanol was introduced into the reaction mixture which was subsequently stirred overnight at room temperature. The modified polymers were precipitated twice into a mixture of anhydrous acetone and diethyl ether (50/50 *v*/v) and dried under vacuum to get white colored products (pHNA and pHNB; yields: 63% and 56% for pHNA and pHNB respectively). Next, the obtained polymers were dissolved in 2 mL dry DMSO and DMAE-CI (3.4 g, 14.4 mmol) was loaded under argon purging. After 72 h reaction at room temperature, the resulting mixture was diluted with 20 mL 2.5 mM ammonium acetate buffer (pH 5) and subsequently ultra-filtrated for 24 h with a membrane MWCO of 3000 Da. The resulting polymer solutions were filtered with 0.2 μm sterile filter before freeze-drying. Yield 57% for pHDA and 71% for pHDB.

2.3.3. RAFT synthesis of the homopolymer of NAS (pNAS)

A typical polymerization procedure for pNAS with a degree of polymerization (DP) of 120 is described in a previously published paper [31]. In short, a reaction vial (8 mL) was charged with NAS (0.5 g, 2.95 mmol) in anhydrous DMF (1.4 mL, 2 M solution) and 4-cyano-4-[(dodecyl-sulfanylthiocarbonyl)sulfanyl]pentanoic acid (5.96 mg, 0.014 mmol) (CTA, CDTPA). A solution of AIBN (24 μL, 0.24 mg, 1.4 μmol) in anhydrous DMF was transferred into the vial. The [M]/[CTA] ratio was 200/1 (mol/mol), whereas the [CTA]/[Initiator] ratio was kept at 10/1 (mol/mol). The mixture was degassed by three freeze–evacuate–thaw cycles and then heated under argon in an oil bath at 70 °C for 7 h. The vial was removed from the oil bath, cooled with ice-water and exposed to air to terminate the polymerization. Finally, a small sample (30 μL) was withdrawn and characterized by ^{1}H NMR

spectroscopy (in DMSO-d_6) to determine the monomer conversion. The polymer was precipitated in anhydrous acetone (50 mL) and recovered by centrifugation. The procedure was repeated three times and the obtained pellet was subsequently dried under vacuum for 24 h (yield: 0.31 g, 58%). The absence of residual monomers in the obtained polymer was confirmed by ^{1}H NMR spectroscopy (in DMSO-d_6). The trithiocarbonate end group of the polymer was removed according to a procedure similar as described in section 2.3.1 [30]. Typically, pNAS (0.25 g, degree of polymerization 116 calculated from the conversion (63%), thus 11.5 μmol of end-groups) and AIBN (94.5 mg, 575.4 μmol, 50 times molar excess over pNAS) were dissolved in anhydrous DMF (2 mL). The solution was heated for 90 min at 80 °C. Subsequently, the homopolymer was precipitated in 100 mL of anhydrous acetone, collected by centrifugation, and dried under vacuum for a period of 24 h (yield: 0.21 g, 83%). The absence of the trithiocarbonate end group was confirmed by GPC analysis (disappearance of the UV absorbance at 309 nm).

2.3.4. Synthesis of p(Man-r-BCN)/p(Gal-r-BCN)

Functionalization of pNAS with mannose and BCN groups was carried out shown in Scheme 3. In detail, 60 mg of pNAS (0.33 mmol of NAS) was dissolved in anhydrous dimethyl sulfoxide (DMSO, 1.2 mL), followed by addition 9 mg of BCN-amine (0.03 mmol, A-10004, Synaffix BV, the Netherlands) and 28 mg of triethylamine (0.27 mmol), and this mixture was stirred at room temperature for 1 h. Then, 118 mg of 3-(2-aminoethylthio) propyl a-D-mannopyranoside (0.39 mmol) and 402 mg of triethylamine (3.97 mmol) were added. The reaction was carried out at 40 °C for 36 h followed by quenching of the unreacted active ester groups with NH_4OH (1 mL) for half an hour and the polymer was subsequently precipitated in 100 mL methanol. The polymer was re-dissolved in water and ultrafiltrated against MilliQ water for 5 h to remove unreacted mannose and BCN-amine. The resulting polymer solution was filtered with 0.2 μm sterile filter and subsequently freeze-dried. The conjugation efficiency was calculated from ^{1}H NMR spectroscopy (91% for the mannose polymer). The same procedure was performed to synthesize of p(Gal-r-BCN) with a 97% galactose conjugation efficiency. The polymer yield was around 85%. The molar ratio of mannose/galactose and BCN into the polymer chain was determined by ^{1}H NMR spectroscopy (Fig. S12) and it was shown that the molar ratio of BCN in the polymers was 8–9% for both polymers, as calculated from the peak intensity ratio of the hydroxyl group protons of sugar (4.97–5.11 ppm, 4H) and methylene protons of BCN ($OCOCH_2$, 4.02 ppm, 2H).

2.4. Characterization of the polymers

The copolymer composition of the different polymers was determined by ^{1}H NMR analysis performed with a Gemini 400 MHz spectrometer (Varian Associates Inc., NMR Instruments, Palo Alto, CA). The polymers were dissolved in D_2O or DMSO-d_6. The molecular weights and molecular weight distributions of the synthesized copolymers pHN and pNAS were determined by gel permeation chromatography (GPC), using two serial PLgel 5 μm MIXED-D columns (Polymer Laboratories, UK) and PEGs of narrow molecular weight distribution as calibration standards. The eluent was DMF containing 10 mM LiCl, the flow rate was 1 mL/min and the temperature was 60 °C. For pHDA and pHDB, the molecular weights and molecular weight distributions were determined by GPC using a Viscotek-GPC max (Viscotek, Oss, the Netherlands) light scattering (λ = 670 nm, right (90°) and low (7°) angle)/viscosimetric detection system, using a ultrahydrogel 2000, 7.8 × 300 mm column in series with a ultrahydrogel 6.0 × 40 mm guard column (Waters) and 0.3 M NaAc, pH 4.4, 30% acetonitrile as eluent [32]. The flow rate was 0.6 mL/min and the run time was 50 min. PolyCALTM PEO standard (M_n = 24 kDa, PDI = 1.01, Malvern) was used for calibration.

2.5. Modification of ovalbumin (OVA) with azide groups

ADDP (7 or 14 μL, 30 mg/mL in dry DMSO) was added to 2.5 mL of OVA (2.5 mg/mL in DPBS, Serva Electrophoresis GmbH) resulting in molar ratios of azide and OVA of 5:1 and 10:1, respectively. The mixtures were incubated for 1 h at room temperature. The modified OVA was subsequently purified with PD 10 column chromatography using nuclease-free water as eluent and subsequently freeze-dried. The number of modified lysine residues was determined by using the TNBS assay (Thermo Fisher Scientific) according to the protocol of the supplier. Sulfo-Cy3 modified OVA was synthesized using the same procedure as for the azide modified OVA with a molar ratio sulfo-cy3/OVA of 2/1.

2.5.1. Spectral analysis of azide modified OVA

UV absorption spectra of 0.5 mg/mL native and modified OVA in DPBS were measured in the range of 250–350 nm using a Shimadzu UV-2450 UV–vis spectrophotometer (Shimadzu Corporation, Kyoto, Japan). UV-CD spectra of 0.5 mg/mL native and modified OVA in DPBS buffer were recorded from 250 to 195 nm using a dual-beam DSM 1000 CD spectropolarimeter (On-Line Instruments Systems, Bogart, USA) using cuvettes with a path length of 0.5 mm. Fluorescence measurements were carried out with Jasco FP8300 Spectrofluorometer (JASCO, Easton, USA). The excitation wavelength was set at 280 nm and the emission spectra were recorded in the range of 300–350 nm. Native and modified OVA were measured at a concentration of 0.1 mg/mL in DPBS.

2.6. Particle preparation and characterization

2.6.1. Preparation of self-crosslinked RNA polyplexes

pHDA and pHDB were dissolved in 10 mM NaAc buffer (pH 5) at 10 mg/mL. As shown in Fig. 2a, RNA polyplexes were prepared by mixing 100 μL of pHDA dissolved in 5 mM NaAc buffer (pH 5) with 100 μL of RNA solution (PolyU or Cy5-mRNA_luc) solution in the same buffer at different N/P molar ratios from 0.2 to 2 and a final fixed RNA concentration of 50 μg/ml. The mixture was vortexed for 5 s and incubated at room temperature for 10 min. To prepare the self-crosslinked (pHDA + pHDB) polyplexes, typically, 100 μL of pHDA dissolved in 5 mM NaAc buffer (N/P ratio of 0.5 mol/mol) was mixed with 100 μL of RNA solution (50 μg/ml). After vortexing for 5 s and equilibration for 10 min, 100 μL of pHDB solution in 5 mM NaAc buffer (N/P ratio of 1.2) was added to the RNA/pHDA polyplex dispersion, followed by vortexing and incubating for 10 min at room temperature. To accelerate the crosslink process, sucrose (final concentration 5%) was added to the resulting (pHDA + pHDB)/RNA polyplexes which were subsequently frozen for one hour at −20 °C and thawed at 4 °C (~ 1 h) [33].

2.6.2. Preparation of RNA (core)-OVA(shell) polyplexes (RO)

The remaining BCN groups of the RNA polyplexes were subjected to further copper-free click conjugation with azide modified OVA to immobilize this antigen onto the surface of the RNA polyplexes. To this end, azide modified OVA (OVA SS 10) was dissolved in 5 mM NaAc buffer (pH 5, 2.5 mg/mL)) and added to the RNA polyplex dispersion (prepared as described in section 2.6.1 at OVA/(OVA + polymer) of 33, 50, 66, 75 and 80%, resulting in (N_3 in OVA)/(remaining BCN groups of the polyplexes) ratios of 0.35, 0.7, 1.4, 2.1 and 2.8 mol/mol, followed by vortexing and incubating at 4 °C for 5 min. The modified polyplexes were frozen in liquid nitrogen and freeze-dried. The resulting RNA-OVA polyplexes are further termed RO_X, with x corresponding with the percentage of OVA added to the formulation. To evaluate the conjugation efficiency of OVA to the RNA polyplexes, azide modified OVA and labeled with Sulfo-Cy3 was used to prepare the formulations. The resulting RNA-OVA polyplexes dispersion was freeze-dried and re-dissolved in DPBS. Next, after 1 h, the unconjugated OVA was removed by Vivaspin® 500 centrifugal filter with a molecular cut-off 300 kDa. The concentration of OVA in the filtrate was measured with UV

spectroscopy (548 nm). The conjugation efficiency (CE) was calculated as follows: CE = (total OVA-OVA in filtrate)/total OVA ×100%. The conjugation efficiency of azide functionalized OVA with RNA polyplexes (50% OVA added) was 87%.

2.6.3. Preparation of virus mimicking particles (VMP)

The RNA-OVA (RO_{50}) polyplexes prepared as described in section 2.6.2 containing 60 μg RNA were dispersed in 600 μL 5 mM NaAc buffer. Next, 20.2 μL p(Man-r-BCN) or p(Gal-r-BCN) (10 mg/mL in water) was added to OVA/RNA polyplexes at (BCN in sugar polymer)/(azide in OVA) molar ratio of 1.2, followed by freeze-drying. The resulting VMPs (VMP-Man/VMP-Gal) were stored at 4 °C and re-suspended in DPBS for further experiments.

2.6.4. Lectin binding assay and stability assay

The ability of the VMP-Man to bind to a mannose-specific lectin was investigated using a Concanavalin A (ConA, 104 kDa, Sigma-Aldrich, the Netherlands) agglutination assay [34]. Sixty μL of VMP-Man dispersion (RNA concentration was 100 μg/mL) in DPBS was pipetted into a DLS microcuvet and subsequently diluted with 240 μL DPBS, containing $CaCl_2$ and $MgCl_2$ (0.901 mM and 0.493 mM, respectively). DLS measurements were recorded every 60 s at room temperature. After 5 min, 300 μL of a 0.5 mg/mL ConA in DPBS was pipetted into the microcuvette under continuous recording of the DLS data. The size was measured for another 10 mins. Analogous to the above-described assay, the interaction of VMP-Gal with Con A was investigated under identical conditions. For stability assay, 1 mL VMP-Man dispersion (RNA concentration 10 μg/mL in DPBS) was pipetted into a microcuvette under and the size of the particles was recorded by DLS for 6 h at 37 °C. The stability of the VMP-Man was also studied under reducing conditions. Therefore, DTT was added to VMP-Man dispersion in DPBS to a final concentration of 10 mM and the size of the particles was recorded by DLS for 6 h at 37 °C.

2.7. Particle size and zeta-potential measurements

The size and size distribution of the polyplexes were measured with DLS using an ALV CGS-3 system (Malvern Instruments, Malvern, UK) equipped with a JDS Uniphase 22 mW He—Ne laser operating at 632.8 nm, an optical fiber-based detector, a digital LV/LSE-5003 correlator with temperature controller set at 25 or 37 °C. The zeta-potential (ζ) of the polyplexes was measured using a Malvern Zetasizer Nano-Z (Malvern, UK) with universal ZEN 1002 'dip' cells and DTS (Nano) software (version 4.20) at 25 or 37 °C. Polyplex measurements were performed in 5 mM HEPES pH 7.4 and at an RNA concentration of 10 μg/mL. For the stability study (section 2.6.4), polyplexes were re-suspended or diluted in DPBS with a final RNA concentration of 10 μg/mL.

2.8. Uptake of RO by DC2.4 cells

DC2.4 cells were seeded into a 48-well plate (70,000 cells/well) and incubated in RPMI-1640 medium (10% HI-FBS, 50 μM 2-mercaptoethanol and 2 mM L-glutamine) for 24 h at 37 °C. RO polyplexes (OVA with Cy3 labeled and RNA (luc_mRNA) with Cy5 labeled) were diluted with cell culture medium to a final OVA concentration of 7.5 μg/mL. Next, the cell medium was changed with 200 μL medium containing the different formulations and incubated for 4 h at 37 °C. The cells were washed with DPBS and 50 μL EDTA (2 mM) was added to detach the cells from the plates. The presence of internalized RO polyplexes was examined by flow cytometry (Canto II, BD). For confocal microscopy, DC 2.4 cells were seeded into 96-well μClear® black plates (10,000 cells/well) and incubated for 24 h at 37 °C. Then, the medium was replaced with fresh medium containing different RO formulations (OVA labeled with Cy3 and RNA labeled with Cy5) at a final OVA concentration of 7.5 μg/mL and the cells were subsequently incubated for another 4 h at 37 °C. Next, the medium was replaced with fresh medium containing Hoechst33342 for staining the nuclei (incubation at 37 °C for 10 min). After washing with DPBS, CLSM images were recorded using Yokogawa CV7000S imager (Yokogawa group, Tokyo, Japan) equipped with a 60× water immersion objective at excitation wavelength of 405, 561 and 646 nm for Hoechst33342, Cy3-OVA and Cy5-RNA, respectively.

2.9. In vitro antigen presentation and cytotoxicity study

2.9.1. MHC class I antigen presentation assay

D2.4 cells (50,000 cells/well) were seeded in a 96-well plate and cultured for 24 h at 37 °C and subsequently incubated with soluble OVA, soluble OVA + polymer (same concentrations of pHDA and pHDB as used to prepare VMP formulations) and VMP at titrated amounts of OVA (12.5–75 μg/mL) for 18 h at 37 °C. Subsequently, B3Z cells (CD8 + T cell hybridoma cells, 50,000 cells/well), in 100 μL IMDM medium (10% HI-FBS, 25 μM 2-mercaptoethanol and 2 mM Glutamax) were added to the D2.4 cells and co-incubated for 24 h at 37 °C. The hybridoma B3Z cells produce β-galactosidase after being activated by DCs that present SIINFEKL in MHC molecules, thus allowing measurement of antigen presentation by a colorimetric assay using β-galactosidase assay (CPRG) [35]. β-Galactosidase activity of B3Z cells was measured by incubating the cells with 100 μL of CPRG buffer for 1 h at 37 °C. β-Galactosidase converts the yellow–orange substrate CPRG into the chromophore chlorophenol red that absorbs at 590 nm, and the absorbance was read by SPECTROstar (BMG Labtech, Ortenberg, Germany). To determine the relative maximum B3Z T cell activation, DCs were loaded with 1 μg/mL of the H-$2K^b$-restricted OVA class I epitope SIINFEKL (Invitrogen) as positive control and the extinction value was set as 100% [13].

2.9.2. Cytotoxicity of VMP formulations

To determine cytotoxicity of VMP formulations, the Alamar Blue cell viability assay (Invitrogen, Karlsruhe, Germany) was performed. In short, 24 h after incubation with the indicated formulations as described above, the cell medium was replaced with culture medium containing Alamar Blue (50 nM) and cultured for another 4 h at 37 °C. Next, 80 μL of medium was transferred into a flat-bottom 96-well plate to measure the light absorbance. The relative cell metabolic activity was calculated by normalizing the absorbance at 570 nm (reference wavelength of 630 nm) with the absorbance of DPBS-treated cells.

2.10. Murine bone marrow derived DCs cellular uptake and maturation

Bone marrow derived DCs (BMDCs) were generated using a protocol as described by Coen et al. [34]. After harvesting BMDC from C57BL/6 mice with 6 days culturing, the cells were pulsed with different VMP formulations (Cy5-luc_mRNA) at an OVA concentration of 7.5 μg/mL. After 1 h of incubation at 37 °C, the cells were detached and transferred into Eppendorf tubes and centrifuged (10 min, 250 × *g*, 4 °C). The supernatant was aspirated, discarded, and the cell pellets were stained with 50 μL L/D –Amcyan/CD11c-PE-Texa-red (BD Biosciences) for 30 mins on ice. Next, 200 μL of FACS buffer (1% BSA in DPBS) was added to the samples prior to centrifugation (10 min, 250 × *g*, 4 °C). The supernatant was aspired, and the cell pellets were suspended in 200 μL of FACS buffer and kept on ice to prevent cell lysis. The cells were then subjected to flow cytometry analysis. To measure the maturation level of the BMDCs, after their incubation with the VMPs for 24 h, the cells were washed with FACS buffer and subsequently stained with an antibody cocktail solution containing L/D-Amcyan, CD11c-PE-Texa-red, CD40-APC and MHCII-FITC antibodies (2 μg/mL, 50 μL per well, eBioscience) for 30 min on ice. The BMDCs were subsequently analyzed by flow cytometry after being washed with FACS buffer. FACS analysis was performed using a BD Accuri C6 (BD Biosciences) and data were processed by FlowJo software.

2.11. Cytotoxic T lymphocyte activity in vivo

Female wild type C57BL/6 mice were purchased from Janvier (Le Genest Saint Isle, France). All mice were 7–12 weeks old at the start of the experiment and maintained under pathogen-free conditions. Subcutaneous immunizations were performed in C57BL/6 mice twice at tail base in a 3 week interval (Fig. 7a). Mice were injected with OVA (InvivoGen), OVA + polymer (same amount of pHDA and pHDB used for the preparation of the VMP formulations), OVA + PolyU polyplexes [36], VMP-Gal and VMP-Man with an OVA dose of 25 μg (plus 5 μg PolyU) in a total volume of 40 μl of 5% glucose in saline RNase-free water (Ambion, Life technologies, USA). Two weeks after boost injection, mice were injected intravenously with 1.5×10^7 target splenocyte cells. Splenocytes were pulsed with 1 μg/ml of MHC-I OVA peptide (SIINFEKL, Invitrogen) or HIV-1 Gag peptide (AnaSpec) as a control before labelling with 5 μM (Termed $CFSE^{hi}$) or 0.5 μM (termed $CFSE^{low}$) 5-(and 6)-carboxyfluorescein diacetate succinimidyl ester (CFSE, Invitrogen), respectively. Labeled cells were mixed at a 1:1 ratio and were adoptively transferred into immunized mice. Two days later, splenocytes from host mice were analyzed by flow cytometry after staining with α-F4/80 (BD Biosciences, San Diego, CA, USA) to exclude autofluorescent macrophages. Percentage antigen-specific killing cells was determined using the following formula: 100–100 * ((% $CFSE^{h}$i cells/% $CFSE^{low}$ cells)$_{immunized\ mice}$/(% $CFSE^{hi}$ cells/% $CFSE^{low}$ cells)$_{non\text{-}immunized\ mice}$.

2.12. Measurement of Ab titers

The mice were immunized as described in section 2.11, and 7 days after the boost administration serum was collected from the mice for antibody titer analyses. To measure the OVA specific Ab titers, 96-well plates were coated with 100 μl OVA (10 μg/mL) in DPBS overnight at 4 °C. The plates were washed (1 × 5 min) with buffer (DPBS containing 0.05% Tween 20) and incubated for 2 h with blocking buffer (DPBS containing 2% BSA and 0.05% Tween 20). Next, the plates were incubated with 5-fold serially diluted serum in blocking buffer starting with a dilution of 1:50 for 2 h. To detect bound Ab, the plates were washed (3 × 5 min) and incubated for 1 h with HRP-conjugated anti-mouse total IgG1and IgG2c Ab (Southern Biotech, Birmingham, USA) with a dilution of 1:3000 in blocking buffer. After the plates were washed (3 × 5 min), 100 μl TMB substrate solution (Sigma-Aldrich, the Netherlands) was added to the wells to initiate the color reaction at room temperature in the dark for 30 min. The reaction was stopped with 2 N H_2SO_4 (50 μL/well), and the OD was measured at a wavelength of 450 nm (OD_{450}).

2.13. Statistical analysis

Unless otherwise mentioned, triplicate data were obtained and presented as mean ± standard deviation. Statistical analysis for comparison between means was performed with software Graphpad Prism 7 and a value of $p < 0.05$ was considered significant.

3. Results and discussion

3.1. Synthesis and characterization of polymers

The building block polymers with azide and BCN functional groups were synthesized as shown in Scheme 2. Firstly, p(HPMA-r-NAS) was synthesized *via* RAFT polymerization using a similar procedure as previously published [29] with 27 mol% of NAS in the copolymer (M_n = 14 kDa, PDI = 1.31) (Fig. S1a). No significant peak shift in the RI chromatogram and decrease of UV absorbance at 309 nm (the absorbance maximum of the trithiocarbonate group [37]) of the polymer before and after incubation with AIBN confirmed the successful removal of the RAFT trithiocarbonate end group (> 92%) (Fig. S1 b&c). Next, the copolymer was reacted either with 2-((2-azidoethyl) disulfanyl) ethan-1-amine hydrochloride (AEDA) or BCN-amine in a 1.2:1 molar ratio relative to the number of NAS units in the copolymer, followed the addition of an excess of 1-amino-propam-2-ol to fully convert remaining unreacted NAS groups (Scheme 2). ^{1}H NMR analysis of the modified polymers after purification showed that the azide and BCN groups were indeed incorporated into the polymers with a conjugation efficiency of 77 and 75%, relative to NAS group (Table 1).

In the last step (Scheme 2), the azide and BCN functionalized polymers were reacted with DMAE-CI to yield the cationic polymers p(HPMA-DMAE-r-AEDA) (pHDA) and p(HPMA-DMAE-r-BCN) (pHDB). After purification of the polymers by ultrafiltration, ^{1}H NMR (Fig. S3 for pHDA and Fig. S4 for pHDB) showed the appearance of a new peak at δ 4.75 ppm (2H, OCH_2CH_2, HPMA-DMAE), confirming the successful reaction of the hydroxyl group of HPMA with DMAE-CI. By comparing the integral ratio of the peak at δ 4.75 ppm and the remaining peak at δ 3.74 ppm (1H, CH_2CHCH_3O, HPMA), it is calculated that the conjugation efficiencies with DMAE-CI are 63 and 68% for pHDA and pHDB, respectively (Table 1). GPC analysis of the final polymers showed that pHDA had a relatively low PDI (1.40) after post-polymerization, while pHDB had a broader molecular weight distribution (PDI of 2.01). This broader molecular weight distribution can likely be ascribed to a side reaction of BCN with the thiol at the ω-end of the polymer by thiol-yne reaction [38,39], because around 10% of the polymer chains still carry a trithiocarbonate group after end group removal, which can be subsequently be converted into a free thiol group by aminolysis during post-polymerization modification [37,40].

3.2. Modification of OVA with azide groups

To covalently conjugate OVA to the RNA polyplexes (Scheme 1), the OVA antigen was modified with azide groups using 3-((2-azidoethyl) disulfanyl) propanoic acid NHS ester (ADDP, Scheme S3) for subsequent coupling with BCN groups present on the particles. The disulfide bond between OVA and particles enables the intracellular release of OVA due to the presence of glutathione (2–10 mM) [41,42]. Varying amounts of azide groups were introduced by reaction of OVA with ADDP at different molar ratio (Fig. 1a). The number of azide groups introduced to OVA was determined by a TNBS assay. This assay determines the number of free lysine residues in proteins and thus the number of lysine per protein reacted with ADDP can be calculated. The results of the TNBS assay show that 1.5 and 3.6 of azide groups per OVA molecule were introduced when ADDP was added at a 5 and 10 molar excess, respectively (Fig. 1a). The maximum modification of 3–4 azide groups is in line with the observation that three of lysine groups are easily accessible in native OVA [43]. The modified OVA was further characterized spectral analysis (Fig. 1b–d). The fluorescence and circular dichroism (CD) spectra showed no significant differences between native and modified protein, which demonstrates that neither aggregation nor significant changes in secondary or tertiary structures occurred after OVA modification. As shown in Fig. 1d, the increase of UV absorbance at 280 nm for the modified OVA might be attributed to the contribution to the absorption of the introduced disulfide bonds [43]. OVA modified with an average of 3.6 azide groups (OVA SS 10, Fig. 1a) was used for the experiments discussed in the following sections.

3.3. Preparation and characterization of RNA-OVA polyplexes

It has been shown in previous studies that the physicochemical properties of polyelectrolyte complexes are dependent on the mixing sequence of the negatively charged polyanion (*e.g.* a nucleic acid) and the cationic polymer [44,45]. As illustrated in Fig. 2a, three steps can be distinguished in the preparation of the RNA (core)-OVA (shell) polyplexes (RO). pHDA was first mixed with RNA (PolyU) to form negatively charged particles (at N/P ratio < 1), followed by coating of

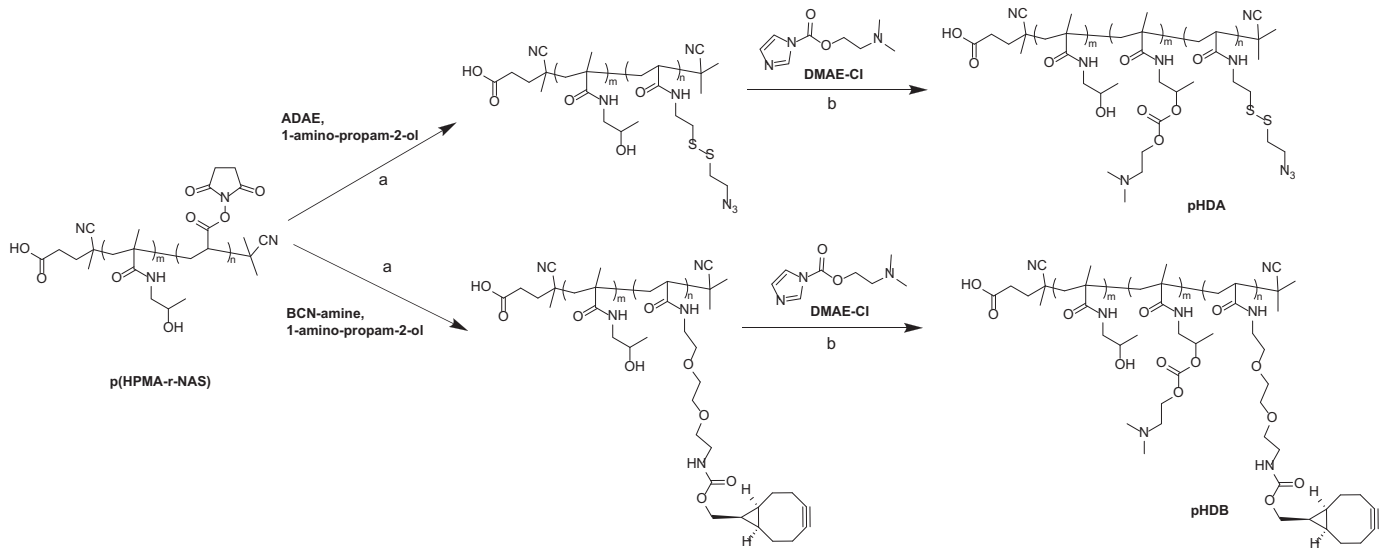

Scheme 2. Post-polymerization modification of p(HPMA-r-NAS) copolymer to yield the azide-containing polymer pHDA and the BCN-containing polymer pHDB: (a) TEA, dry DMSO, 35 °C, 50 h; (b) TEA, DMSO, room temperature, 72 h.

Table 1
Characteristics of the synthesized copolymers used in the present study.

Polymers	Abbreviation	HPMA (% mol)[a]	NAS (% mol)	HPMA-DMAE (% mol)	ADAE/BCN (% mol)	M_n[c](g/mol)	M_w/M_n
P(HPMA-r-NAS)	pHN	72 (62%)[b]	28 (58%) [b]	0	0	14,400	1.31
P(HPMA-DMAE-r-ADAE)	pHDA	26	0	49 (63%)[b]	25 (87%)[b]	21,600	1.40
P(HPMA-DMAE-r-BCN)	pHDB	29	0	53 (68%)[b]	18 (61%)[b]	28,100	2.01

[a] Copolymer composition as determined by ^{1}H NMR.
[b] Conversion (percentage) calculated from ^{1}H NMR.
[c] Determined by GPC viscotek analysis (0.3 M NaAc, pH 4.4, with 30% acetonitrile as eluent).

the formed polyplexes with a slight excess of pHDB to yield positively charged particles. The freeze-thaw treatment likely accelerates the click reaction [33, 36] between azide (from pHDA) and BCN (from pHDB) groups to form the crosslinked RNA core, and the excess amount of BCN groups was subsequently used for conjugation of azide modified OVA to the surface of the particles. It should be noted that the addition of azide modified OVA to these cationic polyplexes (zeta potential was 18 mV) at pH 7.4 (5 mM HEPES buffer) resulted in the formation of aggregates (> 1 μm; Fig. S7) likely because of the highly negative charge (−25 mV) of OVA (pI = 4.9 [46]). The net surface charge of OVA is dependent on the pH of the buffer in which the protein is dissolved, and therefore to decrease the surface charge of OVA, the formulations were prepared in pH 5 ammonium acetate (NH_4OAc, 5 mM) buffer, in which OVA has a slightly positive charge (9 mV). Besides, Stănciuc et al. showed that OVA preserved its immunoreactive epitopes upon incubation at pH 7 and 4.5 even after being heated at 80 °C and denatured [47]. Another advantage of the used NH_4OAc buffer is that this ammonium salt can be evaporated during freeze-drying [48].

To obtain insight into the self-assembling properties (exploiting electrostatic interactions) of pHDA/pHDB and RNA, RNA (PolyU) was mixed with pHDA or pHDB at varying N/P ratios from 0.2 to 1.2, where the N/P ratio refers to the molar ratio of amines (N, cationic groups, $pK_a = 9.5$) in the polymers to phosphates (P, anionic groups, $pK_a < 1$) in the nucleic acid. As shown in Fig. 2b, pHDA formed small negatively charged RNA polyplexes at an N/P ratio of 0.5 (around 60 nm in diameter; zeta potential −32 mV). At this stage, pHDA plays a role as an electrostatic glue and binds the negatively charged RNA, as depicted in step a of Fig. 2a. At an N/P ratio of 0.8, pHDA/RNA aggregates (830 nm, 6 mV) were formed. Positively charged polyplexes with size of < 150 nm were formed at an N/P ratio of 1 and higher. A similar trend was observed for the pHDB/RNA polyplexes (Fig. 2c), in line with the other studies of PEI/DNA [45] and pDMEAEM/DNA polyplexes [49].

To prepare small RNA polyplexes, RNA was first complexed with the azide containing polymer pHDA at an N/P ratio of 0.5 (Fig. 2b). Next, pHDB at different N/P ratios was added to these preformed polyplexes dispersion to find the optimal N/P ratio, at which positively charged polyplexes were formed with low amounts of free pHDB in the polyplex dispersion. As shown in Fig. 2d, after addition of pHDB at an N/P ratio of 1.2 and higher, polyplexes with a size of around 75 nm and positive zeta potential (33 mV) were formed. Agarose gel electrophoresis (Fig. S8) showed that no free RNA was present in the dispersion. The resulting (pHDA(0.5) + pHDB(1.2))/RNA polyplexes were subsequently frozen (−20 °C for 1 h) and thawed (4 °C for 1 h) to accelerate the copper-free click reaction between the azide and BCN groups [33,36], to yield the self-crosslinked RNA core. This freeze/thawing procedure resulted in an increase of size (from 75 to 150 nm), while the zeta potential only showed a slight decrease (from 33 to 30 mV) (Fig. S9a). After incubation with 150 mM NaCl (pH 5, 5 mM NH_4Ac buffer) for 5 h at room temperature, the size of the non-crosslinked pHDB/RNA (N/P = 1.7) polyplexes increased from 180 to 1500 nm, which is normal for cationic polyplexes like PEI/RNA [50]. In contrast, the RNA core showed a limited increase in size from 150 to 450 nm after 5 h incubation (Fig. S9b). This increase can be ascribed to swelling of the RNA polyplexes due to weaker electrostatic interactions and demonstrates that indeed crosslinked polyplexes were formed. It should be noted that the overall BCN (from pHDB) to azide (from pHDA) molar ratio in the RNA polyplexes dispersion was 1.5, and therefore, the resulting crosslinked RNA core still has an excess of BCN groups which are available for further modification.

The prepared RNA/pHDA/pHDB particles were subjected to surface grafting with azide modified OVA (OVA SS 10, Fig. 1a) through copper-

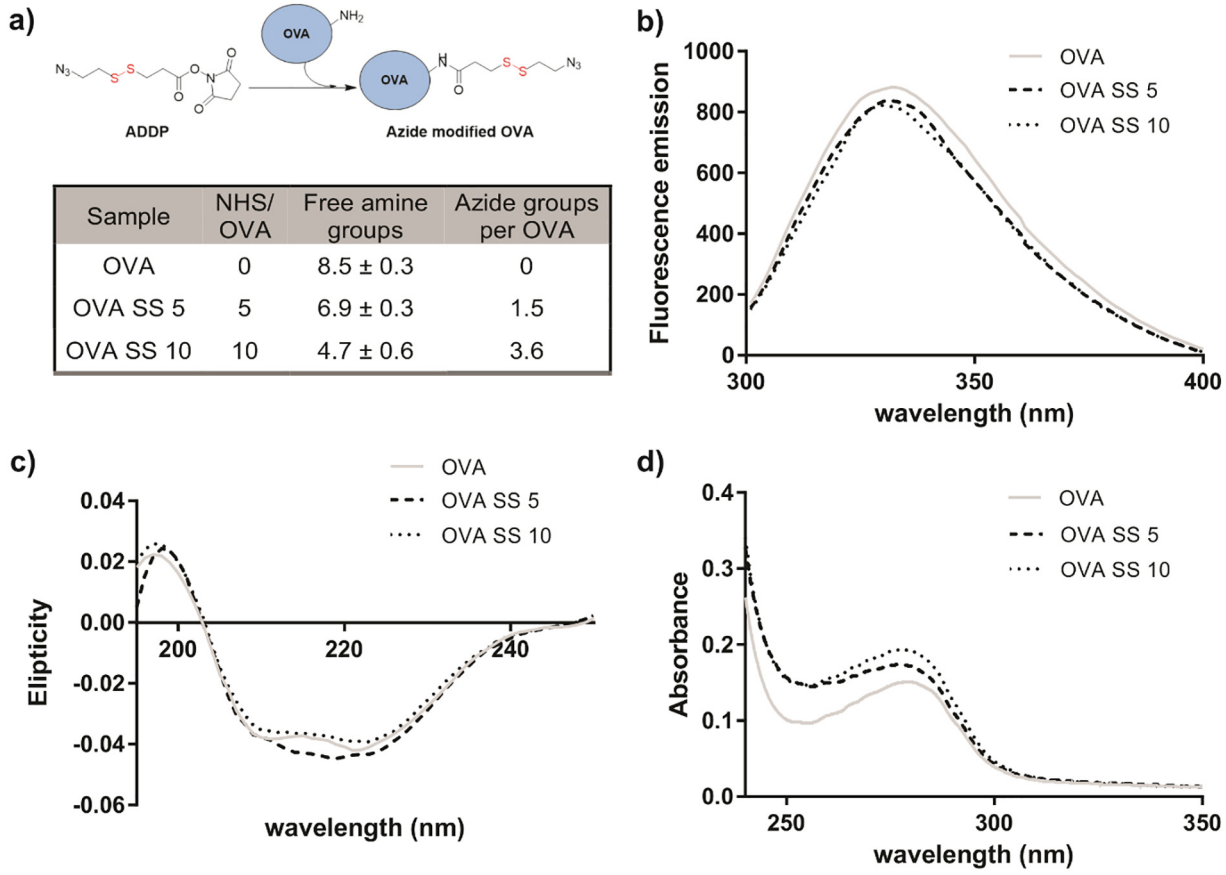

Sample	NHS/ OVA	Free amine groups	Azide groups per OVA
OVA	0	8.5 ± 0.3	0
OVA SS 5	5	6.9 ± 0.3	1.5
OVA SS 10	10	4.7 ± 0.6	3.6

Fig. 1. Characteristics of azide-modified OVA. (a) Table summarizing the number of free amines of OVA as determined by the TNBS assay (n = 3). Fluorescence emission spectra (b), far-UV CD (circular dichroism) spectra (c) and UV–vis spectra of azide-modified OVA samples.

free click conjugation between the azide groups of OVA and remaining BCN moieties of the particles, generating a reducible disulfide bonds between the RNA core and the OVA shell (Fig. 2a, step c). Different ratios of OVA SS10 were mixed with the RNA core dispersions. With an increasing of OVA, the size of the RNA-OVA (RO) polyplexes slightly increased from 145 to 178 nm (Fig. 2e). Regardless of the amount of OVA added, the PDI of particles remained low (< 0.2), indicating that the original structure of RNA polyplexes was maintained after OVA coupling. Fig. 2f shows that a gradual decrease in zeta potential from 36 to 14 mV was observed with an increasing amount of OVA added. As shown in Fig. 2g, the narrow distribution of the RO polyplexes was preserved when 75% weight ratio of OVA was added. To accelerate the conjugation reaction between the azide groups of OVA and the BCN groups, the RO polyplexes were freeze-dried [36]. As shown in Table 2, after freeze-drying and redispersion in 5 mM HEPES buffer, pH 7.4, the RO polyplexes size slightly increased; for example, the size of RO_{50} (refers to 50% OVA loaded particles) increased from 155 to 177 nm. The RO_{75} particles had a slightly bigger size (195 *vs* 177 nm) and a lower zeta potential (−13.3 *vs* − 3.2 mV) as compared to the RO_{50} particles. These negative zeta potential values can be explained by the negative charge of OVA at pH 7.4. It is important to note that OVA conjugation and the freeze-dry treatment did not lead to detectable RNA release or RNA chain scission, as demonstrated by agarose gel electrophoresis (Fig. S8).

The uptake of RO polyplexes by DC 2.4 cells was investigated. The RO polyplexes were prepared by using Cy5-labeled mRNA_luc and sulfo-Cy3 conjugated OVA (sulfo-Cy3-OVA SS 10, Table S1). As shown in Fig. 3a, DC cells took up RO_{50} efficiently and the fluorescence signals from RNA and endocytosed OVA confirmed colocalization, which indicates that RNA (adjuvant) and OVA (antigen) were present the same subcellular compartment. The uptake efficacy of RO polyplexes, soluble OVA and OVA + polymer (OVA was mixed with same amount of polymer used for the preparation of polyplexes) was also studied by confocal microscopy as well as flow cytometry. Strong green fluorescence signals were observed in the DCs incubated with RO polyplexes (both RO_{50} and RO_{75}) compared to the those incubated with soluble OVA and OVA + polymer (Fig. 3b). The percentage of DCs that internalized OVA when incubated with RO_{50} was about two-fold higher as compared to soluble OVA, whereas a similar uptake percentage was observed for OVA + polymer (Fig. 3c). However, the amount of OVA internalized by DCs measured *via* mean fluorescence intensity (MFI) in the Cy5 channel of the RO_{50} formulation was about two times higher than for OVA + polymer (Fig.S10a). The higher cellular uptake of OVA + polymer formulation compared to soluble OVA can probably be ascribed to the formation of micrometer sized particles (Table 2). Likely, the azide modified OVA is conjugated to the BCN moieties of pHDB during the freeze-dry treatment, as studies have shown that the coupling of OVA to a cationic polymer enhances the OVA cellular uptake [51,52]. It should be noticed that although the RO_{50} and RO_{75} particles have around the same particle size (177 and 195 nm, respectively), the cellular uptake of RO_{75} was significantly lower than that of the RO_{50} particles (Fig. 3c), which may be ascribed to the lower zeta potential of the RO_{75} polyplexes (−13 and − 3 mV, respectively, Table 2). Apart from that, the RNA cellular uptake percentage of RO_{50} was around 100%, which was two times higher (MFI, five times higher) than observed for the uptake of RO_{75} (Fig. S10b). Importantly, the RO_{50} instead of RO_{75} polyplexes showed that all DCs that have endocytosed OVA also internalized RNA (Fig. 3c), which is ideal and critical for immune activation and antigen presentation [53, 54]. On the basis of these results, the RO_{50} formulation was selected for further investigations described later.

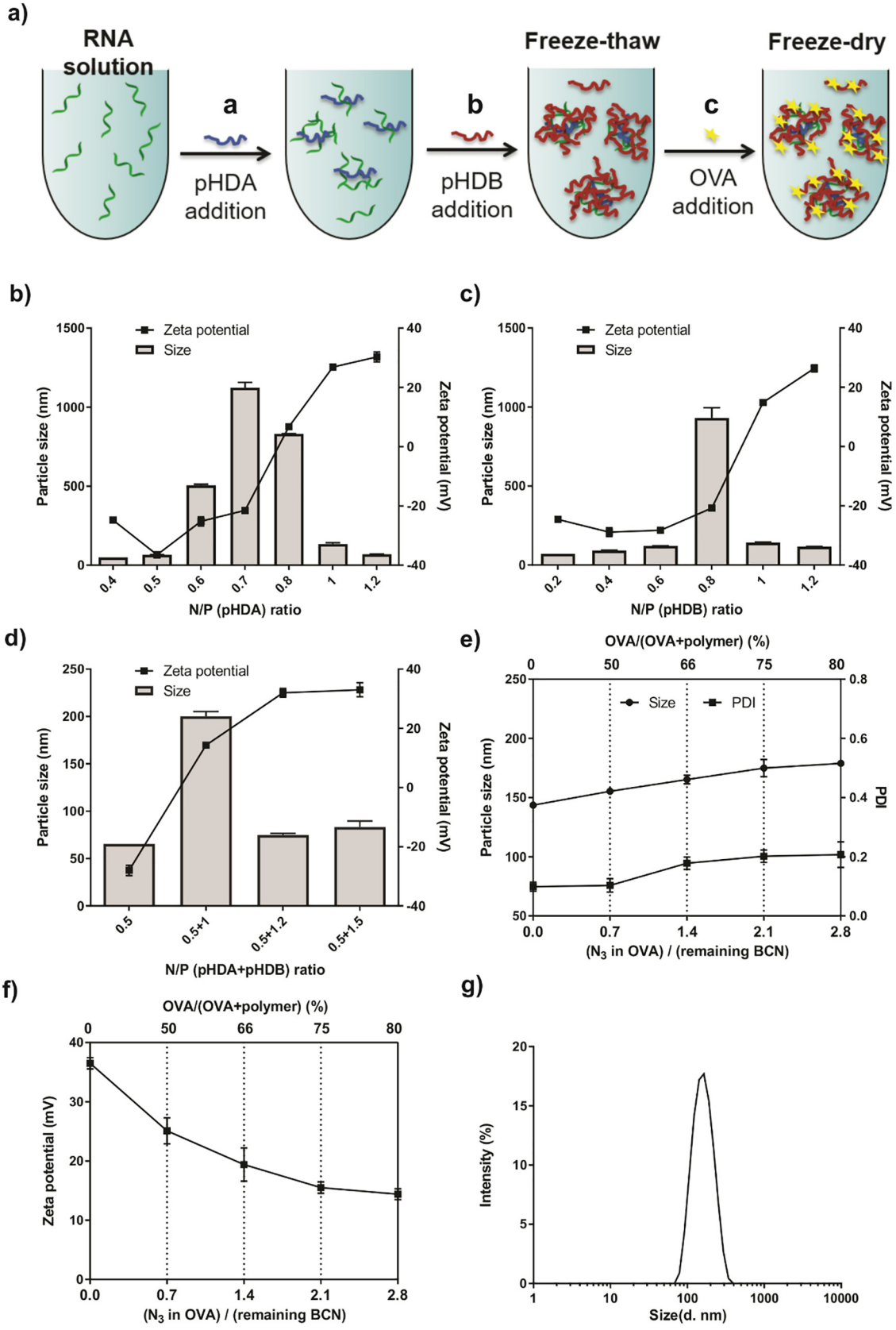

Fig. 2. a) Schematic representation of the preparation of RNA-OVA (RO) polyplexes. Particle size and zeta potential of pHDA/RNA polyplexes (b), pHDB/RNA polyplexes (c) and (pHDA + pHDB)/RNA polyplexes (d) as a function of N/P ratio. Surface modification of RNA core ((pHDA(0.5) + pHDB(1.2))/RNA polyplexes) with azide modified OVA (OVA SS10) at various mixing (N_3 in OVA)/(remaining BCN groups of the polyplexes) ratios to yield RNA-OVA polyplexes, termed as RO. (e) Size and PDI and (f) zeta potential of RO polyplexes. (g) DLS histogram of RO_{75} prepared at (N_3 in OVA)/(remaining BCN groups of the polyplexes) = 2.1, which means 75% weight ratio of OVA added. The polyplexes were prepared in 5 mM NH_4Ac buffer, with a final RNA concentration of 50 μg/mL. Data are presented as mean ± SD.

Table 2
Particle size and zeta potential of polyplexes.

Sample	Before freeze-drying (pH 5)		After freeze-drying (pH 7.4)[b]	
	Z_{ave} (nm)	Zeta potential (mV)	Z_{ave} (nm)	Zeta potential (mV)
RNA core	141 ± 2	33.2 ± 1.5	156 ± 1	16.4 ± 2.2
RO_{50}	155 ± 3	25.2 ± 2.2	177 ± 3	−3.2 ± 0.3
RO_{75}	169 ± 7	15.5 ± 1.4	195 ± 5	−13.3 ± 0.8
OVA + polymer[a]	244 ± 1	20.2 ± 0.8	1263 ± 17	−5.2 ± 0.2

[a] Same amount of OVA SS 10 and (pHDA + pHDB) used to prepare RO_{50}.
[b] Polyplexes were prepared at 5 mM NH_4OAc buffer (pH 5), after freeze-drying, the particles were resuspended in 5 mM HEPES buffer (pH 7.4). mean ± SD are shown.

3.4. Preparation and characterization of virus mimicking particles (VMPs)

To mimic glycans of glycoproteins present on the envelope of viruses (*e.g.* HIV and influenza), a polyvalent copolymer with mannose repeating units and BCN groups in the side chain was synthesized (Scheme 3) and coated on the surface of RO polyplexes to yield virus mimicking particles (VMPs) which potentially can target DCs. Similarly, a polymer modified with galactose and BCN units that likely does not target DCs was also synthesized and used as a non-functionalized control.

First, poly(N-acryloyloxysuccinimide) (pNAS) with a degree of polymerization of 120 was synthesized by RAFT polymerization (PDI = 1.4, Table S2). After removal of the end trithiocarbonate group, pNAS was reacted with either mannose-amine or galactose-amine (Fig. S12) together with BCN-amine (Scheme 3) followed by hydrolysis of the unreacted NAS groups with ammonium hydroxide. The resulting polymers p(Man-r-BCN)/p(Gal-r-BCN) were characterized by ^{1}H NMR (Fig. S12) and GPC analysis (Fig. S13). The results are summarized in Table S2. The resulting p(Man-r-BCN) and p(Gal-r-BCN) showed narrow and unimodal molecular weight distribution (M_n = ~30 kDa).

The p(Man-r-BCN) or p(Gal-r-BCN) were next added to the RO_{50} dispersion at a BCN groups in p(Man-r-BCN)/p(Gal-r-BCN) to azide in OVA molar ratio of 1.2, the resulting mannosylated or galactosylated RO_{50} polyplexes are termed as VMP-Man and VMP-Gal, respectively. We assume that the unreacted azide groups of OVA during preparation of RO polyplexes are available for reaction with BCN moieties of p(Man-r-BCN)/p(Gal-r-BCN). As shown in Table 3, the generated VMPs after freeze-drying and rehydration in DPBS had a size around 200 nm and a negative zeta potential (−14.3 mV). The smaller particle size and lower surface charge of VMPs compared to RO_{50} can be ascribed to surface shielding by p(Man-r-BCN)/p(Gal-r-BCN), confirming that indeed surface coating with glycans had occurred. Dynamic light scattering (DLS) measurements of VMP-Man (Fig. 4a) particles in DPBS at room temperature showed that the particles had an excellent colloidal stability (no significant changes in size and scattering intensity for 6 h). These results show that the surface coating of RO_{50} with poly(mannose) stabilizes the RO_{50} particles. The reduction sensitive property of VMP-Man

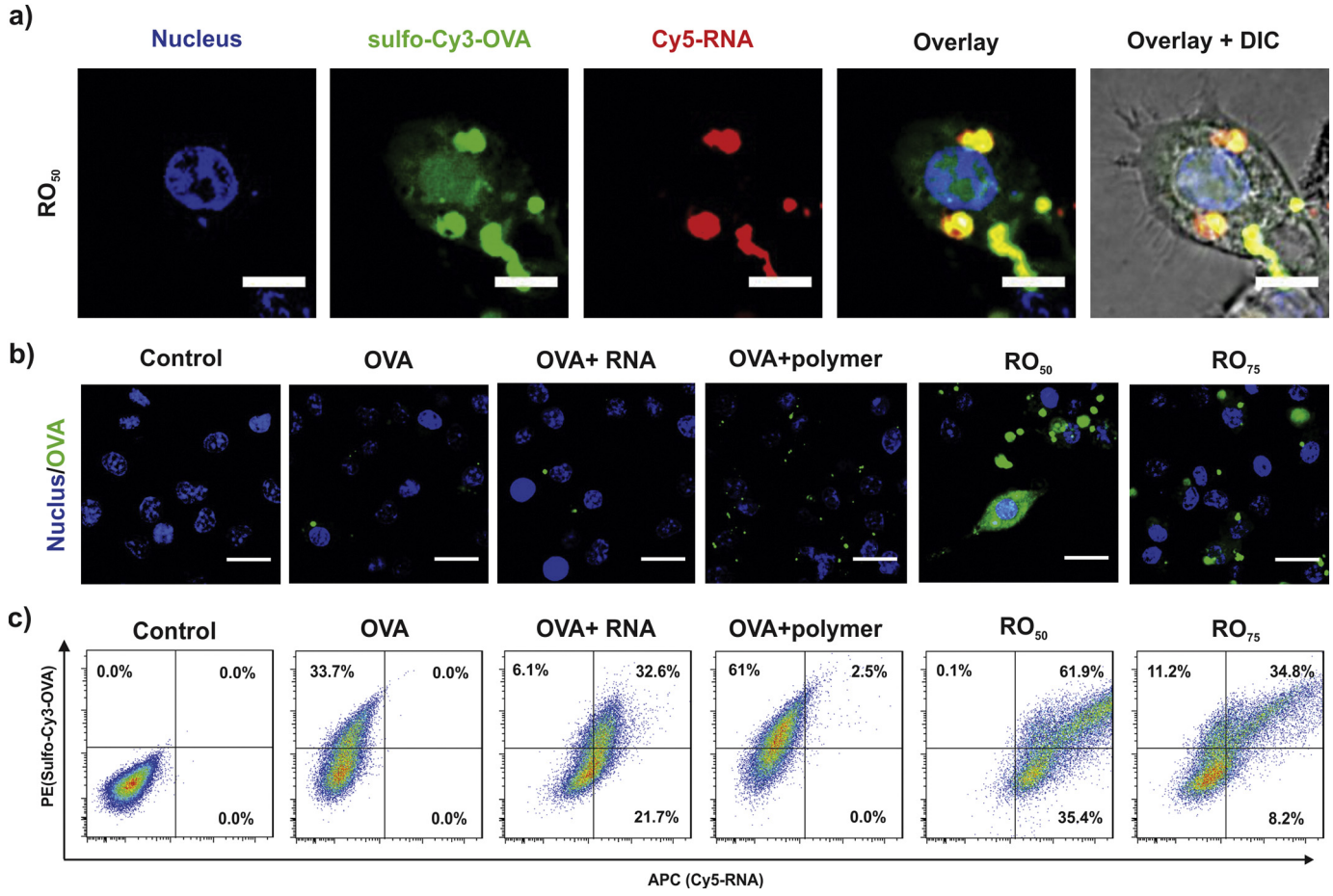

Fig. 3. Co-localization and cellular uptake of RNA-OVA (RO) particles. DC 2.4 cells were incubated with the indicated formulations for 4 h at 37 °C, with a final sulfo-Cy3-OVA (sulfo-Cy3-OVA SS 10, Table S1) concentration of 7.5 μg/mL. (a) representative confocal fluorescence microscopy images of DCs incubated with RO_{50} polyplexes demonstrate the co-localization of the RNA core (Cy5-labeled luc_mRNA) and the OVA shell (labeled with sulfo-Cy3); bar indicates 10 μm. (b) Representative fluorescence microscopy images of indicated formulations (sulfo-Cy3 labeled OVA) after cellular uptake; bar indicates 20 μm. (c) DC 2.4 cells cellular uptake efficiencies of indicated formulations (Cy5-labeled luc_mRNA and sulfo-Cy3 labeled OVA) was analyzed by flow cytometry.

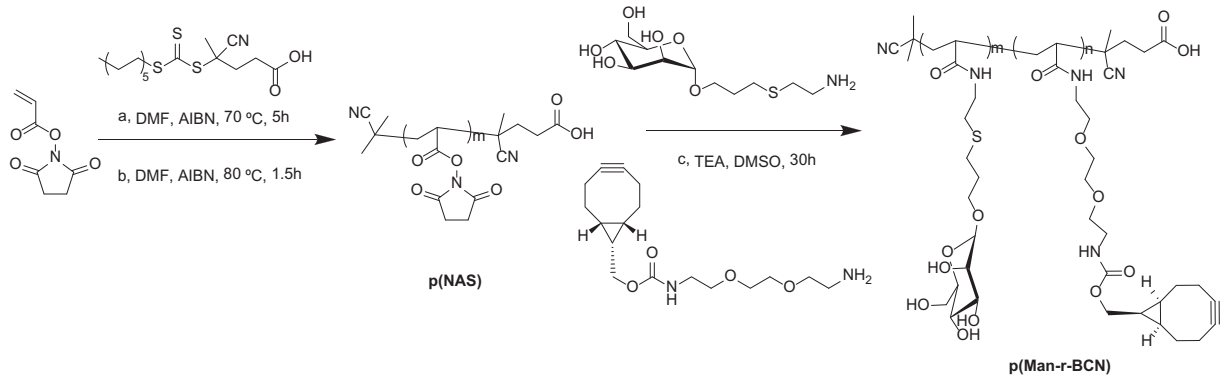

Scheme 3. Synthesis routine of the multivalent polymer p(Man-r-BCN). (a) A homopolymer p(NAS) was first synthesized by RAFT polymerization in dry DMF with CPADB as chain transfer agent and AIBN as initiator; (b) The trithiocarbonate group at ω-end of the polymer was removed using AIBN as the initiating species [55]; (c) p(NAS) was further modified with mannose-NH_2 or galactose-NH_2 and BCN-NH_2 in DMSO to yield the final polymers p(Man-r-BCN) or p(Gla-r-BCN).

Table 3
Particle size and zeta potential of different formulations.

Sample	After freeze-drying and redispersion		
	Z_{ave} (nm)[a]	Zeta potential (mV)[b]	PDI[a]
RO_{50}	504 ± 4	−4.3 ± 1.6	0.097
VMP-Man	198 ± 5	−14.3 ± 1.1	0.196
VMP-Gal	186 ± 4	−15.2 ± 0.5	0.170

[a] Particle size and PDI were measured in DPBS.
[b] Zeta potential was measured in 5 mM HEPES buffer, pH 7.4.

was studied by exposing these particles to DTT (mimicking the intracellular reductive environment) and continuously monitoring their size by DLS. Fig. 4b shows that the light scatting intensity (SLI) gradually decreased during 160 min of incubation while the particle size remained stable (~250 nm). Upon ~150 min of incubation, a rapid decrease in scattering intensity was observed which was associated with a substantial increase in size of the particles. This points to swelling and dissociation of the VMP-Man particles due to reduction of the disulfide bonds that crosslinks the particles. After 300 min incubation, the scattering intensity was low, which implies that most of particles have been dissociated.

The possible exposure of mannose on the surface of the VMP-Man particles was investigated by testing their affinity for concanavalin A (ConA), a lectin that has four binding sites for α-D-mannosyl and α-D-glucosyl residues, but not for α-D-galactosyl residues [56]. As shown in Fig. 4c, after addition of ConA to VMP-Man particles, the size and SLI increased, while no changes were observed for VMP-Gal particles (Fig. 4d). These results convincingly demonstrate that the mannose units were indeed exposed on the surface of VMP-Man particles.

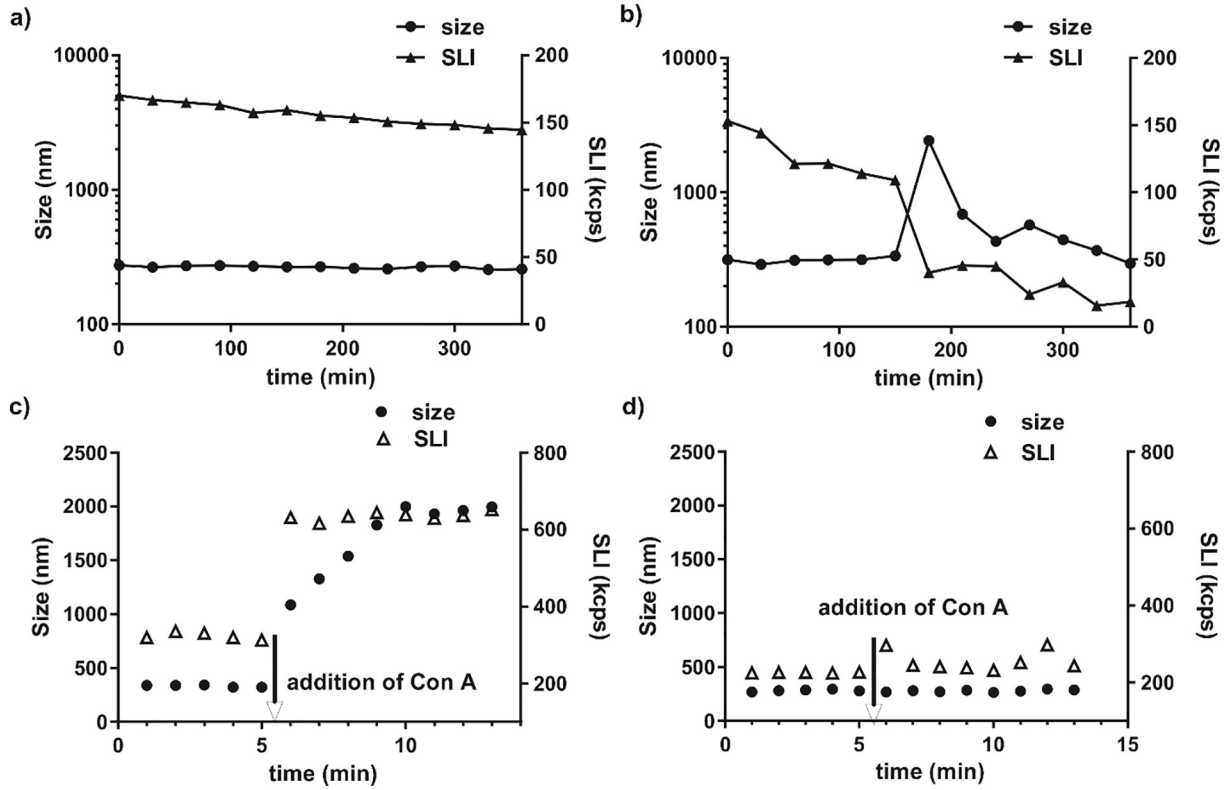

Fig. 4. Particle size and scattered light intensity (SLI) measured by DLS of VMP-Man upon incubation in DPBS in the absence (a) and presence (b) 10 mM DTT at 37 °C. Evolution of size and SLI upon addition of concanavalin A (ConA) to (c) VMP-Man and (d) VMP-Gal particles measured by DLS.

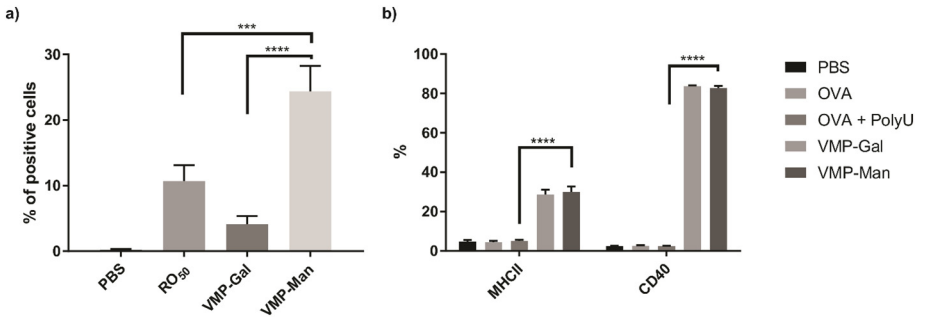

Fig. 5. Flow cytometry analysis of bone-marrow derived DCs (BMDC) cellular uptake efficiency (a) of RO_{50}, VMP-Gal and VMP-Man. The particles formulated with Cy5-mRNA_luc were incubated with BMDC at 37 °C for 1 h. ($n = 3$; $^{**}p < 0.01$; $^{****}p < 0.0001$). (b) Percentage of BMDCs that expressed the maturation makers MHCII and CD40 studied by flow cytometry analysis after incubation of BMDCs with the indicated formulations for 24 h ($n = 4$, $^{****}p < 0.0001$).

3.5. In vitro BMDC cellular uptake and maturation

The potential of VMP-Man particles to specifically target and activate bone marrow derived DCs (BMDCs) was investigated. BMDCs are known to express higher levels of mannose receptor compared to the immortalized cell line DC 2.4 [34]. After 1 h incubation of BMDCs with the different formulations at 37 °C, around 10 and 25% of the cells had taken up the RO_{50} and VMP-Man particles, respectively (Fig. 5a). Importantly, despite having similar particle size (~200 nm) and zeta-potential (−15 mV) as the VMP-Man nanoparticles, VMP-Gal exhibited a 5-fold less association with BMDCs cells, which demonstrates that the uptake of VMP-Man particles indeed mainly occurred *via* mannose-receptor mediated endocytosis.

The capability of VMP-Man/VMP-Gal particles to induce BMDCs maturation was evaluated with flow cytometry by measuring the up-regulation of the co-stimulatory makers CD40 and of MHCII on the surface of DCs after 24 h incubation. As shown in Fig. 5b, soluble OVA with and without soluble PolyU did not exhibit activation of BMDCs. In contrast, the expression of maturation maker MHCII and CD40 was highly increased when BMDCs were incubated with either VMP-Man or VMP-Gal. It has been shown that the synthetic RNA (PolyU) which is loaded in the core the formulation of VMP-man polyplexes, mimics a single chain RNA of viruses, and therefore activates the endosomal toll like receptor TLR7/8 leading to the maturation of DCs [57]. The results proved that the VMPs protect RNA against degradation by RNase in the medium and have the capacity to deliver RNA to the endosome of DC to activate TLR 7/8 after being released from the particles.

3.6. In vitro antigen presentation and cytotoxicity

The potential of the VMP particles to enhance MHC class I antigen cross-presentation was investigated *in vitro* using DC 2.4 cells exploiting the B3Z cell assay [54]. As shown in Fig. 6a, the three different OVA particulate formulations were more efficient in stimulating B3Z T cells

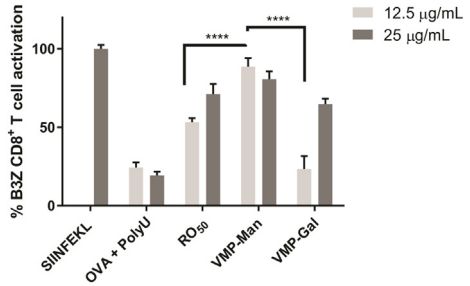

Fig. 6. Efficient MHC class I cross-presentation of VMPs *in vitro*. D2.4 cells were incubated for 24 h with different OVA formulations. MHC class I presentation of processed OVA was detected by co-culture with H-2Kb/SIINFEKL-specific B3Z cells. Normalized values were calculated based on the OD590 nm values obtained by using DC pulsed with SIINFEKL (1 µg/mL) cultured together with B3Z T cells ($OD_{590nm} = 0.84 = 100\%$ CD8+ T cell activation). **** $p < 0.0001$ (two-way ANOVA).

than soluble OVA, due to the enhanced uptake and cross-presentation, as also observed for other particulate OVA delivery systems [58,59]. All three formulations showed similar T cell activation at high OVA concentration (25 µg/ml). However, at low OVA concentration (12.5 µg/ml), VMP-Man showed the highest T cell activation, with a factor of 2–3 higher activation of T cells activation compared with VMP-Gal and 1.5 times higher than RO_{50}. The higher cellular uptake (Fig. 5a) likely contributes to this difference in T cell activation. Importantly, all the formulations did not show any toxicity even at the highest concentration tested (75 µg/mL, Fig. S14).

3.7. In vivo immunogenicity

To investigate to which extent the targeting ability and the enhanced MHC class I presentation of the VMP-Man observed *in vitro* would confer improved antigen specific cellular immune response *in vivo*. Mice were immunized with soluble OVA, VMP-Gal and VMP-Man, following a prime-boost scheme as shown in Fig. 7a. To exclude any intrinisic adjuvant effects of the polymer used to prepare the nanoparticles, mice were immunized with a mixture of soluble OVA and polymer (pHDA + pHDB). For the adjuvant positive control, PEGylated polyplexes loaded with PolyU, which showed strong adjuvant effect in our previous study [36] was used. Cytotoxic T cell responses were assessed using a standard *in vivo* killing assay. Three weeks after the boost immunization, mice were challenged with a 1:1 ratio of OVA peptide-pulsed $CFSE^{hi}$ splenocytes (target cells) and non-pulsed $CFSE^{low}$ splenocytes (non-target cells) (Fig. 7a). Two days after this adoptive transfer, the spleens were isolated and the ratio of target cells *versus* non-target cells was analyzed by flow cytometry. The stronger the evoked cytotoxic T cell response, the more tageted cells are killed, leading to a higher killing percentage. Fig. 7b shows that the mice immunized with the mixture of soluble OVA and polymer exhibited even lower level of antigen specific cell lysis as compared to soluble OVA, indicating the poor adjuvant effects of the soluble polymer used in this study. Immunization with VMP-Gal did not result in antigen specific cell lysis levels above those induced by immunization with antigen in saline. Importantly, The VMP-Man formulation induced the most strongest cytolytic T cell responses. The observed differences in the killing assay between VMP-Man and VMP-Gal can likley be ascribed to the enhanced DC cellular uptake of VMP-Man by binding to the mannose receptors followed by endocytosis and MHC I antigen presentation [60]. On the level of the humoral immune response, VMP-Man strongly promoted IgG1 responses (Fig. 7c), as well as IgG2c (Fig. 7d), which are indicative for the strength of Th1 immunity induction [61]. All formulations with PolyU were potent in eliciting the IgG2c response as compared to soluble OVA [Fig. 7d). A similar phenomenon was observed in previous studies when mice were immuized OVA together with TLR ligands like polyU and resiquimod [13,61-63].Taken together, VMP-Man achieved synergistic effects in terms of effector T cell and humoral responses.

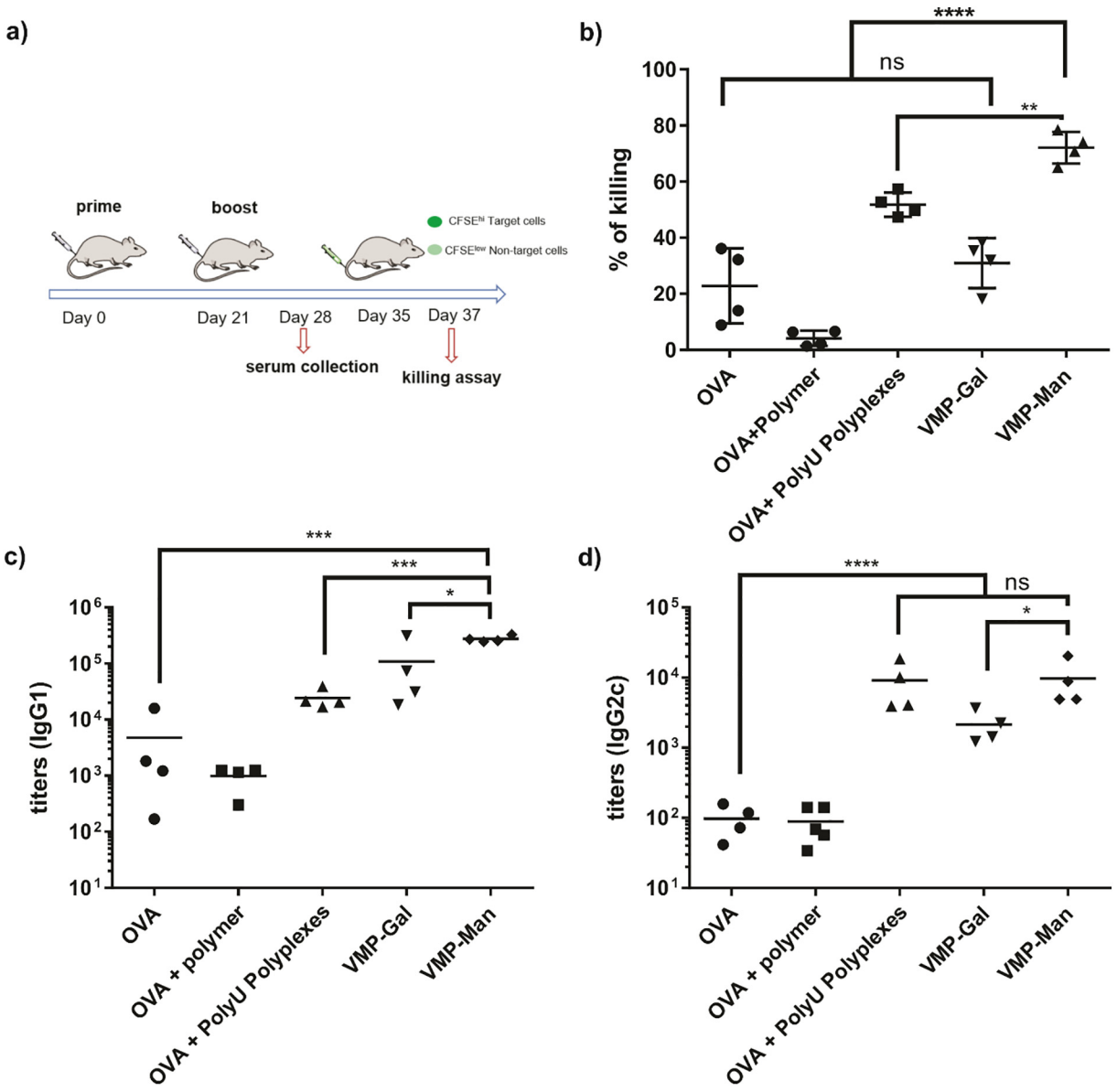

Fig. 7. Adaptive immune responses evoked by VMPs. (a) Schematic representation of the experimental set-up of the immunization protocol. (b) Specific killing of target cells in response to each vaccine formulation. Antibody titers of IgG1 (c) and IgG2c (d) in serum. Data are shown as means of 4 mice/group. *$p < 0.05$; ** $p < 0.01$; ***$p < 0.001$; **** $p < 0.0001$ (one-way ANOVA).

4. Conclusions

In summary, we have developed a virus structure mimicking synthetic vaccine with mannose ligands on the surface, for the effective and simultaneous delivery of an antigen (OVA) and adjuvant (PolyU) to DCs. This reduction-sensitive vaccine can be readily formulated by sequential self-assembly of RNA and OVA with polymers, and followed by surface modification with mannose ligands by employing copper-free click chemistry. The mannosylated VMP-Man particles with a size around 200 nm exhibited enhanced cellular uptake by BMDCs as compared to VMP-Gal and induced DC maturation. VMP-Man had a good cytocompatibility and enabled enhanced MHC I antigen presentation by DCs *in vitro*. Immunization with VMP-Man showed superior antibody and cytolytic T cell responses. In summary, the synthetic VMPs described in this paper are a promising modality to develop vaccines against diseases such as HIV and cancer that require Th1/cytotoxic T cell responses in addition to antibodies for protection.

Conflict of interest

The authors declare no competing financial interest.

Acknowledgements

Bo Lou is financially supported by China Scholarship Council (CSC).

Appendix A. Supplementary data

Supplementary data to this article can be found online at https://doi.org/10.1016/j.jconrel.2018.11.006.

References

[1] T.J. Moyer, A.C. Zmolek, D.J. Irvine, Beyond antigens and adjuvants: formulating future vaccines, J. Clin. Invest. 126 (2016) 799–808.
[2] C. Giefing, A.L. Meinke, M. Hanner, T. Henics, M.D. Bui, D. Gelbmann, U. Lundberg, B.M. Senn, M. Schunn, A. Habel, B. Henriques-Normark, A. Ortqvist, M. Kalin,

A. von Gabain, E. Nagy, Discovery of a novel class of highly conserved vaccine antigens using genomic scale antigenic fingerprinting of pneumococcus with human antibodies, J. Exp. Med. 205 (2008) 117–131.
[3] T.N. Schumacher, R.D. Schreiber, Neoantigens in cancer immunotherapy, Science 348 (2015) 69–74.
[4] T.C. Wirth, F. Kühnel, Neoantigen targeting—Dawn of a new era in cancer immunotherapy? Front. Immunol. 8 (2017) 1848.
[5] R. Arens, T. van Hall, S.H. van der Burg, F. Ossendorp, C.J.M. Melief, Prospects of combinatorial synthetic peptide vaccine-based immunotherapy against cancer, Semin. Immunol. 25 (2013) 182–190.
[6] L. Li, S.P. Goedegebuure, W.E. Gillanders, Preclinical and clinical development of neoantigen vaccines, Ann. Oncol. 28 (2017) xii11–xii17.
[7] A. Pasquale, S. Preiss, F. Silva, N. Garçon, Vaccine Adjuvants: from 1920 to 2015 and beyond, Vaccine 3 (2015) 320–343.
[8] Y. Hailemichael, Z. Dai, N. Jaffarzad, Y. Ye, M.A. Medina, X.-F. Huang, S.M. Dorta-Estremera, N.R. Greeley, G. Nitti, W. Peng, C. Liu, Y. Lou, Z. Wang, W. Ma, B. Rabinovich, R.T. Sowell, K.S. Schluns, R.E. Davis, P. Hwu, W.W. Overwijk, Persistent antigen at vaccination sites induces tumor-specific CD8+ T cell sequestration, dysfunction and deletion, Nat. Med. 19 (2013) 465–472.
[9] J.W. van der Laan, S. Gould, J.Y. Tanir, Safety of vaccine adjuvants: Focus on autoimmunity, Vaccine 33 (2015) 1507–1514.
[10] M.D. Joshi, W.J. Unger, G. Storm, Y. van Kooyk, E. Mastrobattista, Targeting tumor antigens to dendritic cells using particulate carriers, J. Control. Release 161 (2012) 25–37.
[11] L.A. Brito, D.T. O'Hagan, Designing and building the next generation of improved vaccine adjuvants, J. Control. Release 190 (2014) 563–579.
[12] L.J. Cruz, P.J. Tacken, R. Fokkink, B. Joosten, M.C. Stuart, F. Albericio, R. Torensma, C.G. Figdor, Targeted PLGA nano- but not microparticles specifically deliver antigen to human dendritic cells via DC-SIGN in vitro, J. Control. Release 144 (2010) 118–126.
[13] A.L. Silva, R.A. Rosalia, E. Varypataki, S. Sibuea, F. Ossendorp, W. Jiskoot, Poly-(lactic-co-glycolic-acid)-based particulate vaccines: Particle uptake by dendritic cells is a key parameter for immune activation, Vaccine 33 (2015) 847–854.
[14] S. Rahimian, M.F. Fransen, J.W. Kleinovink, M. Amidi, F. Ossendorp, W.E. Hennink, Particulate systems based on poly(Lactic-co-Glycolic)acid (pLGA) for immunotherapy of cancer, Curr. Pharm. Des. 21 (2015) 4201–4216.
[15] S.L. Demento, N. Bonafé, W. Cui, S.M. Kaech, M.J. Caplan, E. Fikrig, M. Ledizet, T.M. Fahmy, TLR9-targeted biodegradable nanoparticles as immunization vectors protect against West Nile encephalitis, J. Immunol. 185 (2010) 2989–2997.
[16] A. Gutjahr, C. Phelip, A.-L. Coolen, C. Monge, A.-S. Boisgard, S. Paul, B. Verrier, Biodegradable polymeric nanoparticles-based vaccine adjuvants for lymph nodes targeting, Vaccine 4 (2016) 34.
[17] D. Li, N. Kordalivand, M.F. Fransen, F. Ossendorp, K. Raemdonck, T. Vermonden, W.E. Hennink, C.F. Van Nostrum, Reduction-sensitive dextran nanogels aimed for intracellular delivery of antigens, Adv. Funct. Mater. 25 (2015) 2993–3003.
[18] Y. Fan, J. Moon, Nanoparticle drug delivery systems designed to improve cancer vaccines and immunotherapy, Vaccine 3 (2015) 662–685.
[19] M. Dierendonck, K. Fierens, R. De Rycke, L. Lybaert, S. Maji, Z. Zhang, Q. Zhang, R. Hoogenboom, B.N. Lambrecht, J. Grooten, J.P. Remon, S. De Koker, B.G. De Geest, Nanoporous hydrogen bonded polymeric microparticles: Facile and economic production of cross presentation promoting vaccine carriers, Adv. Funct. Mater. 24 (2014) 4634–4644.
[20] S. Tandrup Schmidt, C. Foged, K. Smith Korsholm, T. Rades, D. Christensen, Liposome-based adjuvants for subunit vaccines: Formulation strategies for subunit antigens and immunostimulators, Pharmaceutics 8 (2016) 7.
[21] A. Bandyopadhyay, R.L. Fine, S. Demento, L.K. Bockenstedt, T.M. Fahmy, The impact of nanoparticle ligand density on dendritic-cell targeted vaccines, Biomaterials 32 (2011) 3094–3105.
[22] Y.S. Lee, S.W. Kim, Bioreducible polymers for therapeutic gene delivery, J. Control. Release 190 (2014) 424–439.
[23] L. Brülisauer, M.A. Gauthier, J.C. Leroux, Disulfide-containing parenteral delivery systems and their redox-biological fate, J. Control. Release 195 (2014) 147–154.
[24] F. Meng, W.E. Hennink, Z. Zhong, Reduction-sensitive polymers and bioconjugates for biomedical applications, Biomaterials 30 (2009) 2180–2198.
[25] E.D. Goddard-Borger, R.V. Stick, An efficient, inexpensive, and shelf-stable diazotransfer reagent: Imidazole-1-sulfonyl azide hydrochloride, Org. Lett. 9 (2007) 3797–3800.
[26] A.M. Funhoff, C.F. Van Nostrum, A.P.C.A. Janssen, M.H.A.M. Fens, D.J.A. Crommelin, W.E. Hennink, Polymer side-chain degradation as a tool to control the destabilization of polyplexes, Pharm. Res. 21 (2004) 170–176.
[27] N. Vurgun, R.F. Gõmez-Biagi, M. Nitz, Access to versatile β-cyclodextrin scaffolds through guest-mediated monoacylation, Chem. - A Eur. J. 22 (2016) 1062–1069.
[28] F.L. Dufour Menno, Cellulose support containing d-mannose derivatives, (2010) (US20120100097A1).
[29] J. Moraes, I.-M. Simionca, H. Ketari, H.-A. Klok, Avoiding compositional drift during the RAFT copolymerization of N-(2-hydroxypropyl)methacrylamide and N-acryloxysuccinimide: towards uniform platforms for post-polymerization modification, Polym. Chem. 6 (2015) 3245–3251.
[30] M. Chen, G. Moad, E. Rizzardo, Thiocarbonylthio end group removal from RAFT-synthesized polymers by a radical-induced process, J. Polym. Sci. Part A Polym. Chem. 47 (2009) 6704–6714.
[31] Y. Li, J. Yang, B.C. Benicewicz, Well-controlled polymerization of 2-azidoethyl methacrylate at near room temperature and click functionalization, J. Polym. Sci. Part A Polym. Chem. 45 (2007) 4300–4308.
[32] X. Jiang, A. van der Horst, M.J. van Steenbergen, N. Akeroyd, C.F. van Nostrum, P.J. Schoenmakers, W.E. Hennink, Molar-mass characterization of cationic polymers for gene delivery by aqueous size-exclusion chromatography, Pharm. Res. 23 (2006) 595–603.
[33] H. Takemoto, K. Miyata, T. Ishii, S. Hattori, S. Osawa, N. Nishiyama, K. Kataoka, Accelerated polymer − polymer click conjugation by freeze − thaw treatment, Bioconjug. Chem. 23 (2012) 1503–1506.
[34] R. De Coen, N. Vanparijs, M.D.P. Risseeuw, L. Lybaert, B. Louage, S. De Koker, V. Kumar, J. Grooten, L. Taylor, N. Ayres, S. Van Calenbergh, L. Nuhn, B.G. De Geest, PH-Degradable mannosylated nanogels for dendritic cell targeting, Biomacromolecules 17 (2016) 2479–2488.
[35] J. Karttunen, S. Sanderson, N. Shastri, Detection of rare antigen-presenting cells by the lacZ T-cell activation assay suggests an expression cloning strategy for T-cell antigens, Proc. Natl. Acad. Sci. U. S. A. 89 (1992) 6020–6024.
[36] B. Lou, A. De Beuckelaer, G.R. Dakwar, K. Remaut, J. Grooten, K. Braeckmans, B.G. De Geest, E. Mastrobattista, S. De Koker, W.E. Hennink, Post-PEGylated and crosslinked polymeric ssRNA nanocomplexes as adjuvants targeting lymph nodes with increased cytolytic T cell inducing properties, J. Control. Release 284 (2018) 73–83.
[37] H. Willcock, R.K. O'Reilly, End group removal and modification of RAFT polymers, Polym. Chem. 1 (2010) 149–157.
[38] R. van Geel, G.J.M. Pruijn, F.L. van Delft, W.C. Boelens, Preventing thiol-yne addition improves the specificity of strain-promoted azide–alkyne cycloaddition, Bioconjug. Chem. 23 (2012) 392–398.
[39] H. Tian, T.P. Sakmar, T. Huber, A simple method for enhancing the bioorthogonality of cyclooctyne reagent, Chem. Commun. 52 (2016) 5451–5454.
[40] S. Averick, R.A. Mehl, S.R. Das, K. Matyjaszewski, Well-defined biohybrids using reversible-deactivation radical polymerization procedures, J. Control. Release 205 (2015) 45–57.
[41] F.Q. Schafer, G.R. Buettner, Redox environment of the cell as viewed through the redox state of the glutathione disulfide/glutathione couple, Free Radic. Biol. Med. 30 (2001) 1191–1212.
[42] M.J. Heffernan, N. Murthy, Disulfide-crosslinked polyion micelles for delivery of protein therapeutics, Ann. Biomed. Eng. 37 (2009) 1993–2002.
[43] F.S. Steven, G.R. Tristram, The reactivity of free amino groups in native and denatured ovalbumin towards fluorodinitrobenzene, Biochem. J. 70 (1958) 179–182.
[44] C. Schatz, J.M. Lucas, C. Viton, A. Domard, C. Pichot, T. Delair, Formation and properties of positively charged colloids based on polyelectrolyte complexes of biopolymers, Langmuir 20 (2004) 7766–7778.
[45] S.K. Cho, C. Dang, X. Wang, R. Ragan, Y.J. Kwon, Mixing-sequence-dependent nucleic acid complexation and gene transfer efficiency by polyethylenimine, Biomater. Sci. 3 (2015) 1124–1133.
[46] S.A. Kidwai, A.A. Ansari, A. Salahuddin, Effect of succinylation (3-Carboxypropionylation) on the conformation and imunological activity of ovalbumin, Biochem. J. 155 (1976) 171–180.
[47] N. Stănciuc, I. Banu, M. Turturică, I. Aprodu, pH and heat induced structural changes of chicken ovalbumin in relation with antigenic properties, Int. J. Biol. Macromol. 93 ((2016) 572–581.
[48] F. Franks, Freeze-drying of bioproducts: putting principles into practice, Eur. J. Pharm. Biopharm. 45 (1998) 221–229.
[49] J.Y. Cherng, P. Van De Wetering, H. Talsma, D.J.A. Crommelin, W.E. Hennink, Effect of size and serum proteins on transfection efficiency of poly ((2-dimethylamino)ethyl methacrylate)-plasmid nanoparticles, Pharm. Res. 13 (1996) 1038–1042.
[50] Z. Wang, H. Zou, Z. Wang, J. Wu, Z. Xia, M. Feng, Highly stable polyglutamate derivatives/siRNA polyplex efficiently down-relegate survivin expression and augment the efficacy of cisplatin, Int. J. Pharm. 505 (2016) 24–34.
[51] L. Lybaert, N. Vanparijs, K. Fierens, M. Schuijs, L. Nuhn, B.N. Lambrecht, B.G. De Geest, A generic polymer-protein ligation strategy for vaccine delivery, Biomacromolecules 17 (2016) 874–881.
[52] B. Slütter, P.C. Soema, Z. Ding, R. Verheul, W.E. Hennink, W. Jiskoot, Conjugation of ovalbumin to trimethyl chitosan improves immunogenicity of the antigen, J. Control. Release 143 (2010) 207–214.
[53] G. Zhu, F. Zhang, Q. Ni, G. Niu, X. Chen, Efficient nanovaccine delivery in cancer immunotherapy, ACS Nano 11 (2017) 2387–2392.
[54] R. Kuai, L.J. Ochyl, K.S. Bahjat, A. Schwendeman, J.J. Moon, Designer vaccine nanodiscs for personalized cancer immunotherapy, Nat. Mater. 16 (2016) 489–496.
[55] K.V. Gujraty, M.J. Yanjarappa, A. Saraph, A. Joshi, J. Mogridge, R.S. Kane, Synthesis of homopolymers and copolymers containing an active ester of acrylic acid by RAFT: Scaffolds for controlling polyvalent ligand display, J. Polym. Sci. Part A Polym. Chem. 46 (2008) 7249–7257.
[56] D.A. Mann, M. Kanai, D.J. Maly, L.L. Kiessling, Probing low affinity and multivalent interactions with surface plasmon resonance: Ligands for concanavalin A, J. Am. Chem. Soc. 120 (1998) 10575–10582.
[57] S.S. Diebold, T. Kaisho, H. Hemmi, S. Akira, C. Reis E Sousa, Innate antiviral responses by means of TLR7-mediated recognition of single-stranded RNA, Science 303 (2004) 1529–1531 80-.
[58] N. Benne, J. van Duijn, J. Kuiper, W. Jiskoot, B. Slütter, Orchestrating immune responses: how size, shape and rigidity affect the immunogenicity of particulate vaccines, J. Control. Release 234 (2016) 124–134.
[59] A. Gomes, M. Mohsen, M. Bachmann, Harnessing nanoparticles for immunomodulation and vaccines, Vaccine 5 (2017) 6.
[60] S. Burgdorf, A. Kautz, V. Böhnert, P.A. Knolle, C. Kurts, Distinct pathways of antigen uptake, Science 612 (2007) 612–616.
[61] G.M. Lynn, R. Laga, P.A. Darrah, A.S. Ishizuka, A.J. Balaci, A.E. Dulcey, M. Pechar, R. Pola, M.Y. Gerner, A. Yamamoto, C.R. Buechler, K.M. Quinn, M.G. Smelkinson, O. Vanek, R. Cawood, T. Hills, O. Vasalatiy, K. Kastenmüller, J.R. Francica, L. Stutts, J.K. Tom, K.A. Ryu, A.P. Esser-Kahn, T. Etrych, K.D. Fisher, L.W. Seymour,

R.A. Seder, In vivo characterization of the physicochemical properties of polymer-linked TLR agonists that enhance vaccine immunogenicity, Nat. Biotechnol. 33 (2015) 1201–1210.

[62] L. Nuhn, N. Vanparijs, A. De Beuckelaer, L. Lybaert, G. Verstraete, K. Deswarte, S. Lienenklaus, N.M. Shukla, A.C.D. Salyer, B.N. Lambrecht, J. Grooten, S.A. David, S. De Koker, B.G. De Geest, pH-degradable imidazoquinoline-ligated nanogels for lymph node-focused immune activation, Proc. Natl. Acad. Sci. 113 (2016) 8098–8103.

[63] R. Heidenreich, E. Jasny, A. Kowalczyk, J. Lutz, J. Probst, P. Baumhof, B. Scheel, S. Voss, K.J. Kallen, M. Fotin-Mleczek, A novel RNA-based adjuvant combines strong immunostimulatory capacities with a favorable safety profile, Int. J. Cancer 137 (2015) 372–384.